

**DOKUZ EYLÜL UNIVERSITY
GRADUATE SCHOOL OF NATURAL AND APPLIED
SCIENCES**

**DEVELOPING 3 DIMENSIONAL IMAGE
ANALYSIS METHODS FOR
CHARACTERIZATION AND CLASSIFICATION
OF AGGREGATES**

**by
Mahmut SİNECEN**

**July, 2011
İZMİR**

**DEVELOPING 3 DIMENSIONAL IMAGE
ANALYSIS METHODS FOR
CHARACTERIZATION AND CLASSIFICATION
OF AGGREGATES**

**A Thesis Submitted to the
Graduate School of Natural and Applied Sciences of Dokuz Eylül University
In Partial Fulfillment of the Requirements for the Degree of Doctor of
Philosophy in Electrical and Electronics Engineering,
Applied Electrical and Electronics Program**

**by
Mahmut SİNECEN**

**July, 2011
İZMİR**

Ph.D. THESIS EXAMINATION RESULT FORM

We have read the thesis entitled “DEVELOPING 3 DIMENSIONAL IMAGE ANALYSIS METHODS FOR CHARACTERIZATION AND CLASSIFICATION OF AGGREGATES” completed by MAHMUT SİNECEN under supervision of ASSIST. PROF. DR. METEHAN MAKİNACI and we certify that in our opinion it is fully adequate, in scope and in quality, as a thesis for the degree of Doctor of Philosophy.



Assist. Prof. Dr. Metehan MAKİNACI

Supervisor



Assist. Prof. Dr. Haldun SARNEL

Thesis Committee Member



Assist. Prof. Dr. Adil ALPKOÇAK

Thesis Committee Member



Assist. Prof. Dr. İbrahim TÜRKYILMAZ

Examining Committee Member



Assoc. Prof. Dr. Halit YAZICI

Examining Committee Member

Prof. Dr. Mustafa SABUNCU

Director

Graduate School of Natural and Applied Sciences

ACKNOWLEDGMENTS

Initially, I would like to thank to my advisor Assist. Prof. Dr. Metehan MAKİNACI for his guidance, valuable insights, support, experiences, advices and encouragement at every stage of this dissertation. It has been a great honor for me to work with Assist. Prof. Dr. Metehan MAKİNACI.

I would like to thank to the members of my Thesis Progress Committee Assist. Prof. Dr. Adil ALPKOÇAK and Assist. Prof. Dr. Haldun SARNEL for their useful comments, suggestions, trust, and support.

I also would like to thank to Assist. Prof. Dr. Ali TOPAL and his wife for their valuable comments, trust, support and suggestions about aggregates.

I want to thank to my parents, Saime and Ferit SİNECEN, to my sisters, Ayşe YILMAZ and Neşe SİNECEN, and to my brother, Instructor Osman SİNECEN for their trust, encouragement and support throughout my life.

Finally, I specially want to thank to my wife, Fatma SİNECEN. I will not be able to complete this thesis without her supporting, encouraging, helping, trusting and understanding approach.

Mahmut SİNECEN

**DEVELOPING 3 DIMENSIONAL IMAGE ANALYSIS METHODS FOR
DETERMINING CHARACTERISTIC AND CLASSIFICATION OF
AGGREGATES**

ABSTRACT

In this thesis, an interdisciplinary study is presented. In this study, a method for three-dimensional (3D) shape characterization and classification is proposed for the six different aggregates. In the first phase, a new 3D laser based imaging system is designed to capture images of aggregates. The imaging system has been optimized to minimize the errors during image capturing. In the second phase, novel 3D shape characterization parameters of the aggregates are extracted. Geometrical parameters of the aggregates are calculated in 3D spatial domain. The last phase, the aggregates are classified by using different classifier models (ANN, FLDA and KNN) with the help of these parameters. Among the classifier types, multi-layer perceptron neural network model that has two hidden layers gives the best performance that is 99.20 percent. The performance of the proposed system is evaluated using manual measurement method and two-dimensional image processing method. Results are analyzed and compared with other studies given in the literature.

Keywords: Aggregate, three-dimensional imaging system, characterization, classification

AGREGALARIN SINIFLANDIRILMASI VE KARAKTERİZE EDİLMESİ İÇİN ÜÇ BOYUTLU GÖRÜNTÜ ANALİZ METOTLARI GELİŞTİRME

ÖZ

Bu tezde, disiplinler arası bir çalışma sunulmuştur. Bu çalışmada, altı farklı agrega türü için üç-boyutlu (3B) şekil karakterizasyonu ve sınıflandırılması sunulmuştur. İlk aşamada, agrega görüntülerini çekmek için yeni bir 3B lazer tabanlı görüntüleme sistemi oluşturulmuştur. Görüntüleme sistemi görüntü alımı sırasında yaşanan sorunları minimize etmek için optimize edilmiştir. İkinci aşamada, agregaları karakterize eden yeni 3B şekil parametrelerini elde etmek amaçlanmıştır. Agregaların geometrik parametreleri 3B uzamsal düzlemde hesaplanmıştır. Son aşamada, agregalar bu parametreler yardımıyla farklı sınıflandırıcılarda (YSS, FLAA ve KNN) sınıflandırılmıştır. Bu sınıflandırıcı türlerinden en iyi başarımı (yüzde 99.20) veren çok katmanlı algılayıcı sinir ağı modelidir. Amaçlanan sistemin performansı elle ölçüm ve iki-boyutlu (2B) görüntü işleme yöntemleri kullanılarak değerlendirilmiştir. Sonuçlar literatürdeki çalışmalar ile karşılaştırılmış ve analiz edilmiştir.

Anahtar Kelimeler: Agrega, üç-boyutlu görüntüleme sistemi, karakterizasyon, sınıflandırma

CONTENTS

PhD. THESIS EXAMINATION RESULT FORM	ii
ACKNOWLEDGEMENTS	iii
ABSTRACT	iv
ÖZ	vi
CHAPTER ONE - INTRODUCTION	1
1.1 The Problem Statement	1
1.2 Measurement of the Physical Properties of Aggregate	2
1.2.1 Traditional Methods	2
1.2.2 Derived Features Using Digital Image Processing Methods	3
1.3 Literature Review	6
1.4 Goal and Contributions	9
1.5 Organization	9
CHAPTER TWO - AGGREGATES	10
2.1 What is Aggregate?	10
2.2 Shape and Texture Definitions of Aggregates	16
2.2.1 Aggregates Shape	16
2.2.1.1 Aspect Ratio (Rc)	20
2.2.1.2 Rugosity (Rg)	20
2.2.1.3 Radius Ratio (Ry)	21
2.2.1.4 % Rectangle Area (%DA)	21
2.2.1.5 Convexity (C)	22
2.2.1.6 Roundness	23
2.2.2 Aggregate Texture	25
2.2.3 Aggregate Size and Shape Measurement by Using Digital Image Processing	25

CHAPTER THREE - 3D IMAGE PROCESSING	27
3.1 Introduction	27
3.2 3D Imaging-Related Issues	28
3.2.1 Digital Image Processing (DIP)	28
3.2.2 Computer Graphics (CG)	29
3.2.3 Computer Vision (CV)	30
3.2.4 Pattern Recognition (PR)	30
3.3 3D Data Acquisition	32
3.3.1 Laser Ranging System	32
3.3.2 Structural Light Method	32
3.3.3 Moirè Fringe Method	33
3.3.4 Shape from Shading Method	34
3.3.5 Passive Stereoscopic Method	35
3.3.6 Active Stereoscopic Method	35
3.4 3D Imaging Techniques	35
3.4.1 Time-of-Flight (ToF) Technique	35
3.4.2 Triangulation Technique	36
3.4.3 Interferometry Technique	36
3.5 Dynamic 3D-Vision	37
CHAPTER FOUR - MATERIAL AND METHODS	38
4.1 Introduction	38
4.2 Material	38
4.3 Method	39
4.3.1 Manual Measurement Method	40
4.3.2 Two-Dimensional Method	44
4.3.2.1 Imaging System	45
4.3.2.2 Preprocessing	46
4.3.2.3 Feature Extraction	49
4.3.3 Three-Dimensional Method	50
4.3.3.1 Imaging System	52

4.3.3.2 Calibration.....	55
4.3.3.3 Image Preprocessing	56
4.3.3.4 Feature Extraction	59
4.4 Classification.....	66
4.4.1 Multi layer perceptron (MLP).....	66
4.4.2 Radial Basis Function (RBF) network	67
4.4.3 Fisher Linear Discriminant Analysis	67
4.4.4 K-Nearest Neighbor	67
4.5 Results and Discussion.....	71
CHAPTER FIVE - CONCLUSIONS AND SUGGESTIONS FOR FUTURE	
WORK.....	78
5.1 Conclusions.....	78
5.2 Suggestions for Future Work	80
REFERENCES.....	81

CHAPTER ONE

INTRODUCTION

1.1 The Problem Statement

Aggregates, which occupy approximately 75-85 percent of the total volume of concrete, affect the performance of fresh and hardened concrete. Shape and texture characteristics of aggregate are important for workability, reliability, bleeding, pumpability and segregation of concrete.

Classical methods, like sieving or screening, are too inefficient for extracting shape parameters of aggregates. Moreover, they have many disadvantages such as; time consumption, dependence on laboratory conditions, their results may change from person to person. In addition, they do not provide any true measurement of the size of aggregates because of calculating cumulative weight of aggregates.

The image analysis methods are concerned with obtaining information from images. The pictorial information is extracted from captured objects on the screen by using digital image processing techniques. These two-dimensional data, which is derived from three-dimensional real world, is used for classifying objects. In some conditions, 3D data (depth information), which belong to geometrical properties of object, are necessary to do accurate classification.

Many properties of concrete depend on the 3D shape of aggregates. Traditional methods do not give a complete 3D shape characterization and analysis. The aim of this thesis is to develop quantitative 3D image analysis methods for characterization and classification of aggregates.

1.2 Measurement of the Physical Properties of Aggregate

Shape, angularity and texture are the key geometrical properties that are frequently used to characterize aggregates. However, these properties have significant effects on the performance of construction materials such as concrete and asphalt pavements. There is no established and accepted general test method for determination of the geometrical properties of aggregates.

1.2.1 Traditional Methods

The texture and shape characteristics of aggregates are becoming important issues for affecting performance of both Asphalt Concrete (AC) and Portland Cement Concrete (PCC) (Barksdale R. , 1991), (Dilek, 2000), (Galloway, 1994), (Kwan, Mora, & Chan, 1999), (Mora & Kwan, 2000), (Lanaro & Tolppanen, 2002). In addition, physical properties of aggregates are extremely important in terms of cement paste requirement and workability of fresh concrete. Cement paste fills the gaps among aggregates and acts as a binder that holds aggregates together. Moreover, it allows fresh concrete to mix better and has an effect on workability and durability of concrete to various reasons. Staying within the limits of water to cement (W/C) ratio means less cement paste and more durable concrete (Fernlund, Zimmerman, & Kragic, 2007), (Erdogan, et al., 2006).

The physical properties of aggregates can be tested by using different methods such as EN 933, ASTM C1252, ASTM D3398, ASTM D4791, and Indian Standard (IS-2386). These manual test methods that are laborious, time consuming depend on laboratory conditions, and the results may change from person to person and greatly affected the features of the aggregates (Quiroga & Fowler, 2004).

Two different devices are shown in Figure 1.1. EN 933 is a standard about tests for geometrical properties of aggregates. It was accepted by Institute of Turkish Standard in January 2003. Shape Index Gauge is used to determine the shape factor,

Length Gauge is used for elongated aggregates (if length of aggregate is more than 1.8 cm, it is called long), Flakiness Gauge is used for flaky aggregates (if thickness of aggregate is less than 0.6 cm, it is called flaky) (Anonymous, UTEST Material Testing Equipment, 2011). The uncompacted void content of a fine aggregate is determined by using ASTM C1252. This method indicates the angularity, sphericity and workability of a fine aggregate mixture (Anonymous, ASTM International Standards Worldwide - Home, 2011), (Anonymous, Integrated Publishing, 2011).

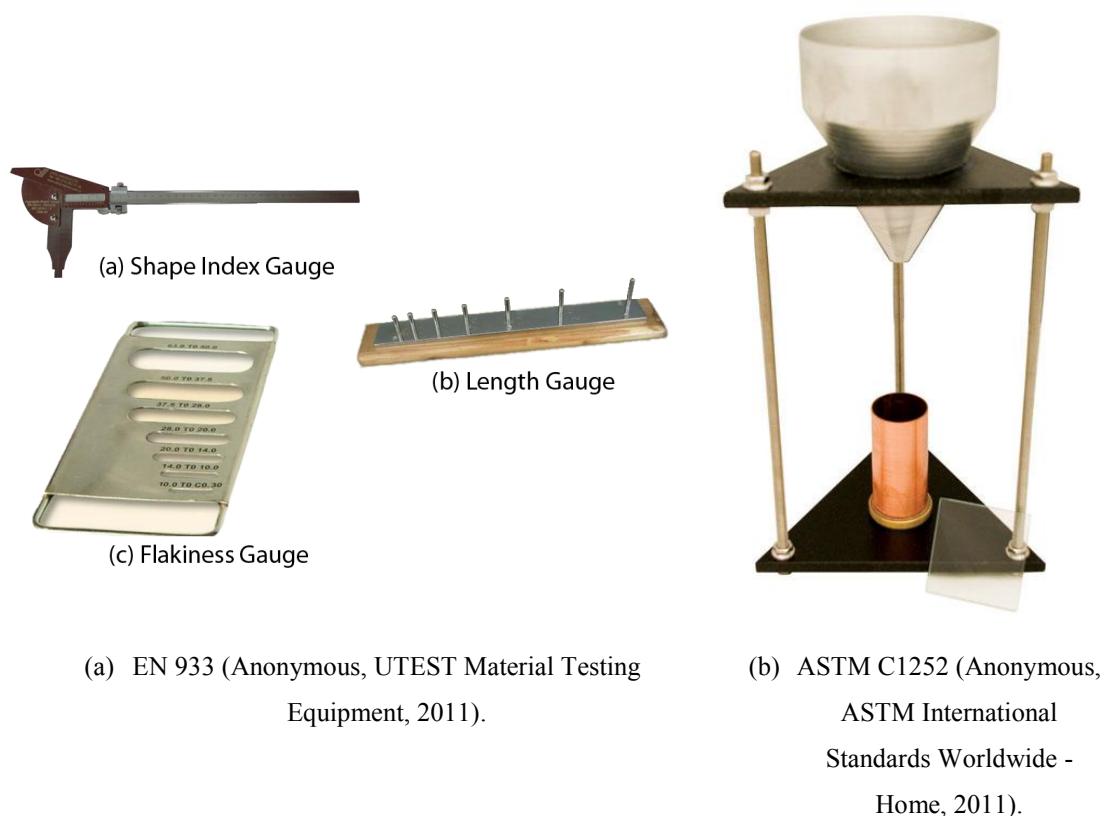


Figure 1.1 Device of manual measurement of aggregate.

1.2.2 Derived Features Using Digital Image Processing Methods

Aggregate geometry is very complex, so even simple, manual experiments cannot be fully explained. Particle geometry also requires very complex definition. Therefore, some simplifications are necessary to summarize shape parameters that are used in aggregate analysis. These shape parameter (feature) definitions are given in the following pages (Equations 1.1-1.13).

- Sphericity (Galloway, 1994)

$$Sphericity = \sqrt[3]{\frac{thickness * width}{length^2}} \quad (1.1)$$

- Shape Factor (Hudson, 1995)

$$Shape Factor = \frac{length * height}{width^2} \quad (1.2)$$

- Length Factor (Kwan, Mora, & Chan, 1999)

$$Length Factor = \frac{width}{length} \quad (1.3)$$

- Flatness Factor (Kwan, Mora, & Chan, 1999)

$$Flatness Factor = \frac{height}{width} \quad (1.4)$$

- Roundness (Kwan, Mora, & Chan, 1999)

$$Roundness = \frac{perimeter^2}{4 * \pi * area} \quad (1.5)$$

- Form Factor (Kuo, Rollings, & Lynch, 1998)

$$Form Factor = \frac{4 * \pi * area}{perimeter^2} \quad (1.6)$$

- Angularity (Kwan, Mora, & Chan, 1999)

$$Angularity = \sum \frac{\left(\frac{\text{average diameter} * r}{\text{radius}}\right)}{N} \quad (1.7)$$

- Front Ratio (Ellipse that is drawn round of aggregate) (Dilek, 2000)

$$Front Ratio = \frac{\text{Minority Axe}}{\text{Majority Axe}} \quad (1.8)$$

- Roughness (Dilek, 2000)

$$Roughness = \frac{\text{perimeter}}{2 * (\text{rectangular (width + height)})} \quad (1.9)$$

- Radius Ratio (Dilek, 2000)

$$Radius Ratio = \frac{\text{Big radius}}{\text{Small radius}} \quad (1.10)$$

- Rectangular Area Ratio (Dilek, 2000)

$$Rectengular Area Ratio = \frac{\text{area}}{\text{small rectangular area}} \quad (1.11)$$

- Concave (Garboczi, 2002)

$$Concave = \frac{\text{Convex area}}{\text{area}} \quad (1.12)$$

- Convexity (Garboczi, 2002)

$$Convexity = \frac{\text{area}}{\text{Convex area}} \quad (1.13)$$

Recent technological advances (in camera optics, CCD cameras and laser rangefinders), availability of high performance computers and low cost imaging systems support the usage of image analysis methods for quantitative measurement of aggregate shape and surface texture properties (Nichols & Lange, 2006), (Jähne, Haussecker, & Geissler, 1999), (Kim, Haas, & Rauch, 2003), (Gonzalez & Woods, 2002), (Russ, 2002). By the way, modern image analysis systems have been developed by through advances in digital imaging devices and computers help to process and store large amount of data at the same time. In this way, the physical properties (diameter, height, width, perimeter, etc.) of aggregate particles can be measured in a much shorter time and aggregates can be classified correctly (Quiroga & Fowler, 2004).

The measurement on three different axes of a particle indicates sphericity. Forms are based on the ratio of long, intermediate and short axis of a particle and a measure of the relation among the three dimensions. As shown Figure 1.2, main dimensions of a particle are Long (L), Intermediate (I) and Short (S).

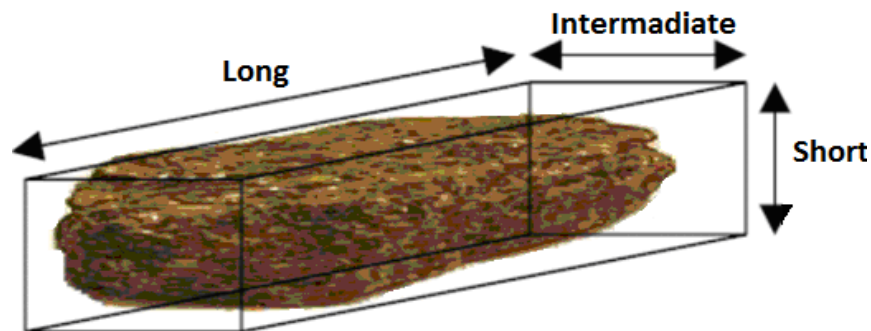
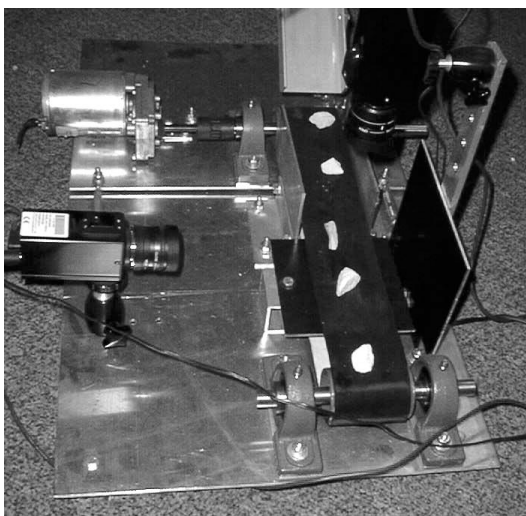


Figure 1.2 Principal dimensions of an aggregate (Haas, Rauch, Kim, & Browne, 2002).

1.3 Literature Review

In recent years, two dimensional (2D) and three-dimensional (3D) image analysis techniques have been used for shape and surface characteristics measurement of aggregate particles. Recent work is summarized in the following paragraph.

Isa, Al-Batah, Zamli, Azizli, Jore, & Noor (2008) used image processing techniques for computing the features such as area and perimeter of aggregate particles. Their study is about Hu's and Zernike's moments related to aggregates. They used image processing methods and artificial neural networks models to find best definition for the features of aggregates. Maerz (1998) used shape measuring system with top and side view of aggregate (Figure 1.3). Mora & Kwan (2000) calculated size properties of three different types of aggregates by using image processing techniques and compared the results by sieve analysis. Lanora & Tolppanen, (2002) used 3D laser scanning system as shown in Figure 1.4 for determining a total 3D geometry of aggregate. Kim, Haas, & Rauch, (2002) used Laser Aggregate Scanning System (LASS) for acquiring 3D data on stone particles. They extracted features using wavelet transforms of the 3D data (Figure 1.5). Wang (2006) calculated shape and size features of aggregates by using image processing techniques by best Ferret methods and compared the results with sieve analysis methods. Fernuld (2005) calculated length, width and thickness features by capturing images of aggregate in lying and standing positions and searched relationship between those features. Lee, Smith, & Smith (2007) calculated shape and form properties of rough aggregates by using 3D image analysis methods. Al-Batah, Isa, Zamli, Sani, & Azizli, (2009) classified aggregates having six different shape types (cubical, angular, irregular, flaky, elongated, flaky elongated) by using artificial neural networks which have different learning algorithms. Itoh, Matsuo, Oida, Miyasaka, & Izumi, (2008) captured image of 7.14 mm, 14.3 mm, 25.4 mm, 25.4 mm, 34.9 mm and 44.5 mm size of aggregates in 22 different lighting levels and measured properties of aggregate shape by using image analysis techniques. Al-Rousan, Masad, Tutumluer, & Tongyan (2007) calculated form, texture and angularity of aggregate by using image analysis techniques and found that these properties were useful to define the characteristics of aggregates. Erdogan, et al. (2006) aimed to find 3D shape properties of aggregates using laser detection and ranging (LADAR). They compared length, width and thickness values obtained from LADAR and X-Ray CT methods and indicated benefits of using LADAR.



(a) Top View



(b) Side View

Figure 1.3 Sample of shape measurement system (Maerz, 1998).



Figure 1.4 Sample of three-dimensional measurement system (Lanaro & Tolppanen, 2002).

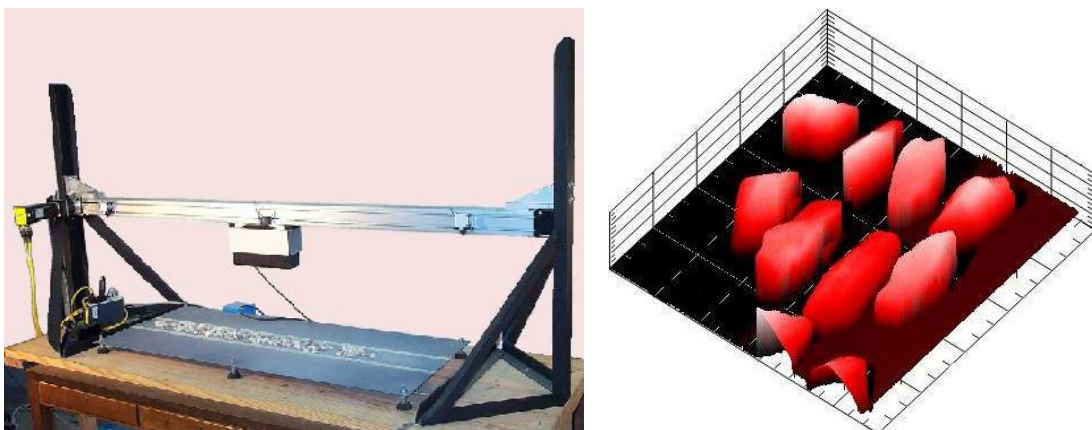


Figure 1.5 Sample of three-dimensional measurement system (Kim, Rauch, & Haas, 2002).

1.4 Goal and Contributions

The goal of this research is to determine the three-dimensional geometrical properties of aggregates and is to classify them into elongate, sphere, round, flat, angular and formless groups. To accomplish this goal, an automated system is designed to aid the civil engineers. Aggregates can be automatically analyzed and classified with this computer-controlled system. It is fast, easier to use and has low error rate than traditional methods.

The main contributions of this work are:

- In this work, an interdisciplinary approach that combines the knowledge from civil engineering and electrical electronics engineering is presented.
- Some new geometrical definitions for morphological properties of aggregate are presented for measurement and classification of aggregates.
- Considering hardware and software implementations, developed measurement device is easy to use, fast, autonomous and has low error rates.

1.5 Organization

The rest of the dissertation is organized as follows:

- The Second Chapter, “What is Aggregate?”, gives information about aggregates.
- The Third Chapter, “3D Imaging Systems”, 3D imaging techniques in the literature are summarized.
- The Fourth Chapter, “Materials and Methodology”, explains materials used and the methods developed.
- The Fifth Chapter, “Results and Future Work”, gives information about future levels of this work, evaluates the results and presents new contributions.

CHAPTER TWO

AGGREGATES

2.1 What is Aggregate?

Aggregates, which are the natural and artificial inert granular materials such as; sand, gravel or crushed stone, occupy approximately 75-85 % volume of concrete (Figure 2.1) (Erdoğan, 2002) (Anonymous, Aggregate, 2011).



Figure 2.1 Aggregate samples.

Characteristics of aggregates affect performance and cost of concrete (Maerz, 1998). The shape of aggregates change amount of paste (water/cement) such as; non-uniform aggregates require more paste. Within the limits of water to cement (W/C) ratio, it means less cement paste and more durable concrete (Quiroga & Fowler, 2004), (Ugurlu, 1999). One or more of the following properties of aggregates affect concrete durability;

- Gradation,
- Maximum aggregate size,
- Shape and surface texture of the particles,
- Unit weight,
- Specific gravity,
- Water absorption,
- Elasticity,
- Thermal properties.

Aggregate size measurement is an important issue because it affects the performance and cost of concrete. Sieve method, which is called gradation test, is used to measure particle size. Sieve method contains more than one sieve with wire mesh screen (Figure 2.2 and Figure 2.3) and is placed in a mechanical shaker (Figure 2.4). Each sieve has smaller screen openings than the one above. Weighed aggregate samples are poured into the top sieve, and shake for specific time (about 10 minutes). After that, retaining aggregate on each sieve is weighed (Figure 2.5) and divided by the total weight as shown in Equation 2.1. Total passing aggregate is found by using Equation 2.2 (Anonymous, Sieve Analysis, 2011).

$$\% \text{ Retained} = \frac{W_{\text{Sieve}}}{W_{\text{Total}}} * 100\% \quad (2.1)$$

$$\% \text{ Passing} = 100\% - \% \text{ Retained} \quad (2.2)$$

Where W_{Sieve} : retaining aggregate weight on each sieve,

W_{Total} : the total weight of aggregate.



Figure 2.2 Sieves samples (Anonymous, Gradation Test, 2011).



Figure 2.3 Stacked sieves used for a gradation and size test (Anonymous, Gradation Test, 2011).



Figure 2.4 Mechanical shaker used for sieve analysis.
(Anonymous, Gradation Test, 2011).

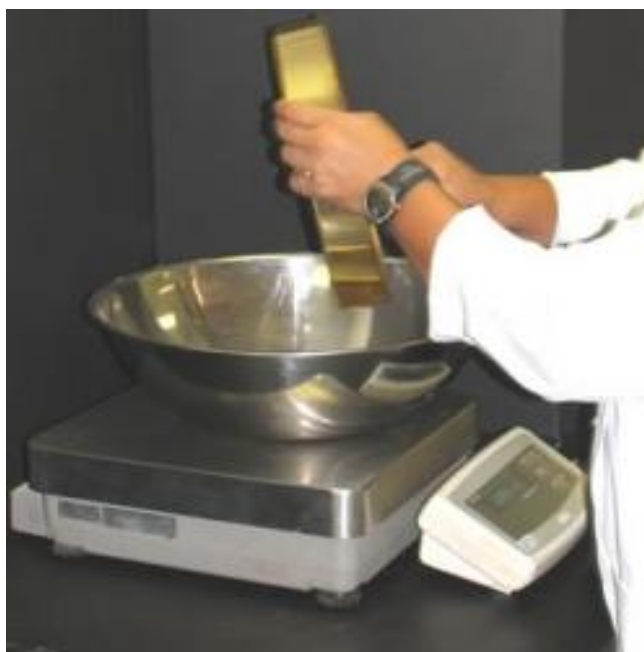


Figure 2.5 Weighing the aggregate retained on a sieve
(Anonymous, Gradation Test, 2011).

Aggregate gradation type is identified with the result of sieve analysis and procedure is outlined in the American Society for Testing and Materials (ASTM) C 136.

Table 2.1 Minimum mass of sample for sieving analysis according to BS812:Part 103:1985.

Nominal size of material (mm)	Minimum mass of sample to be tested (kg)
63.0	50
50.0	35
40.0	15
28.0	5
20.0	2
14.0	1
10.0	0.5
3.0-6.0	0.2
<3.0	0.1

This test has some disadvantages;

- Sieve analysis connects to aggregate sizes because of being standard sieve opening sizes as shown in Table 2.1 (coarse material sizes range down to 150 μm) (Anonymous, Sieve Analysis, 2011),
- Wet and dry materials have different weight (Anonymous, Sieve Analysis, 2011),
- This method assumes that all aggregate are round, which may not be, as shown in Figure 2.5.

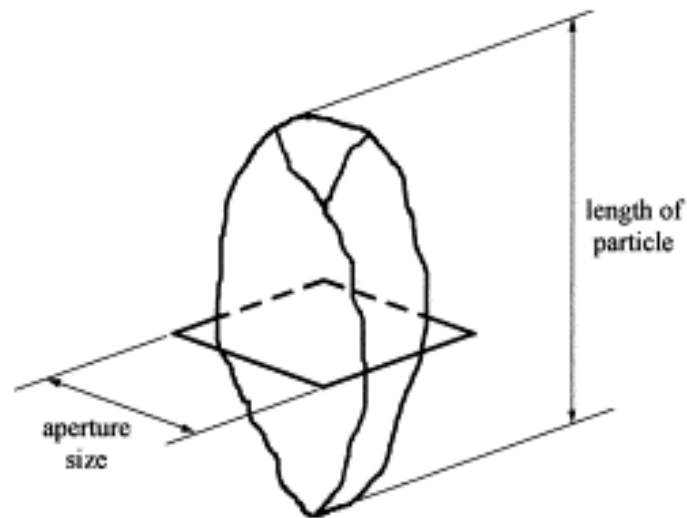


Figure 2.6 An elongated particle passing through a square sieve aperture (Mora & Kwan, 2000).

Two methods used for analyzing shape are ASTM (Aggregate Shape Evaluation) and PN (Polish Standard). They used to measure aggregate shape parameter, such as flakiness, elongation index, and angularity number is measured by Indian standard IS-2386(I), ASTM D4791 is used for flat and elongated aggregates, ASTM D2488, BS812 for measuring angularity (Das, 2006). These methods have disadvantages that are being slow, manual, prone to human errors, etc.

New image processing methods and computer technologies give us new opportunities for aggregate measurements. These methods are faster and more accurate than traditional methods. Studies of image analysis on size and shape measuring of aggregates are many and they are macro and micro scaling size and shape studies in specific laboratories.

2.2 Shape and Texture Definitions of Aggregates

2.2.1 Aggregates Shape

Aggregate geometry is very complex, so even simple experiments cannot be explained fully. Particle geometry requires very complex definition. Therefore, some simplifications must be made. For this purpose, shape must be defined using both sphericity and surface texture model. Sphericity depends on relationship among three main sizes, Length (L), Width (W) and Height (H). Surface texture indicates surface roughness and texture of particle (Brzezichi & Kasperkiewicz, 1999).

Shape, roundness and surface texture are shown on aggregate particle in Figure 2.7 (Kuo & Freeman, 2000). According to that figure; shape represents whole of particle, roundness relates to corner angle of particle and surface structure is a measure of surface texture and roughness of particle.

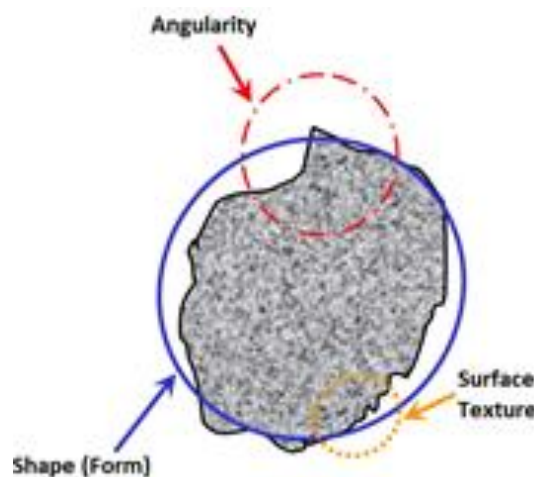


Figure 2.7 Aggregate particle shape (form), angularity and surface texture properties (Kuo & Freeman, 2000).

In the literature, there are many different definitions about aggregate particle shape and surface texture. Sometimes, they are described by using mathematical

expressions, sample figures and table of comparison (Janoo, 1998), (Persson, 1998), (Dilek, 2000), (Mora & Kwan, 2000), (MacLeod, 2002).

Descriptive terms related to aggregates form are given in ASTM D2488 “Standard Practice for Description and Identification of Soils (Visual-Manual Procedure)” as shown in Figure 2.8. Another shape classification of aggregates particle is also given in BS812 “Testing aggregates, Methods for determination of particle size and shape” such as Rounded, Irregular, Angular and Flat.

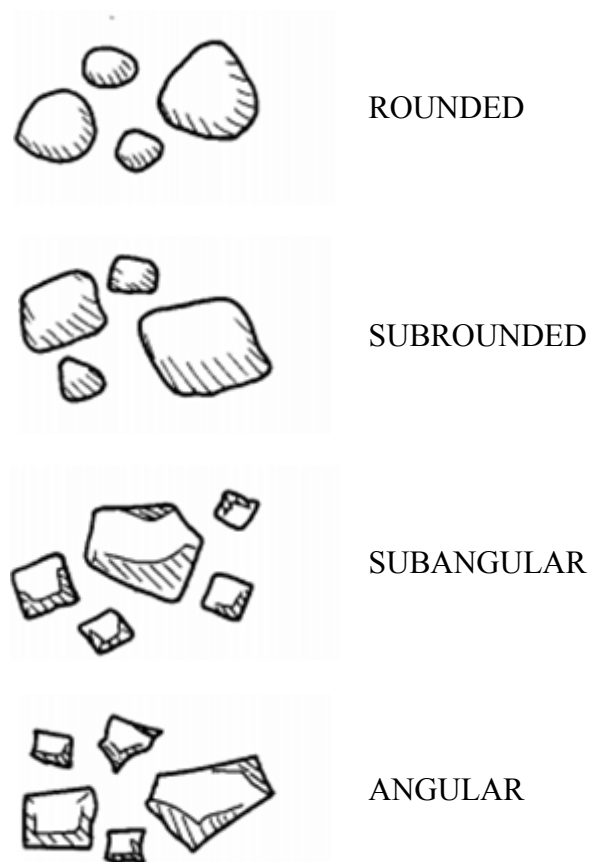


Figure 2.8 Angularity of coarse aggregate particles (Neville, 1995).

The shape of aggregate particles can be described by using two principal properties: „sphericity“ and „roundness“ (Topal, 2001) (Tam, 2007). Aggregate particles are classified as flaky when they have a thickness (smaller dimension) of less than 0.6 of their mean sieve size. Aggregate particles are also classified as

elongated when they have a length (greatest dimension) of more than 1.8 of their mean sieve size according to BS 812 (Part 105.2, 1989). BS 882 also provides limits for the flakiness index (particle thickness relative to other dimensions). Flaky and elongated particles could lead to low workability of fresh concrete, bleeding water accumulation under the aggregate, causing planes of weakness, higher water demand in fresh concrete, lower strength and durability problems in hardened concrete (Topal, 2008).

Sphericity measures what three different axes or size of a particle level equivalent. Forms are based on ratio of dimensions of long, intermediate and short axis of a particle and a measure of the relation among the three dimensions. As shown in Figure 2.9, main dimensions of a particle are Long (L), Intermediate (I) and Short (S), and, sphericity is given by Equation 2.3 (Al-Rousan, 2004).

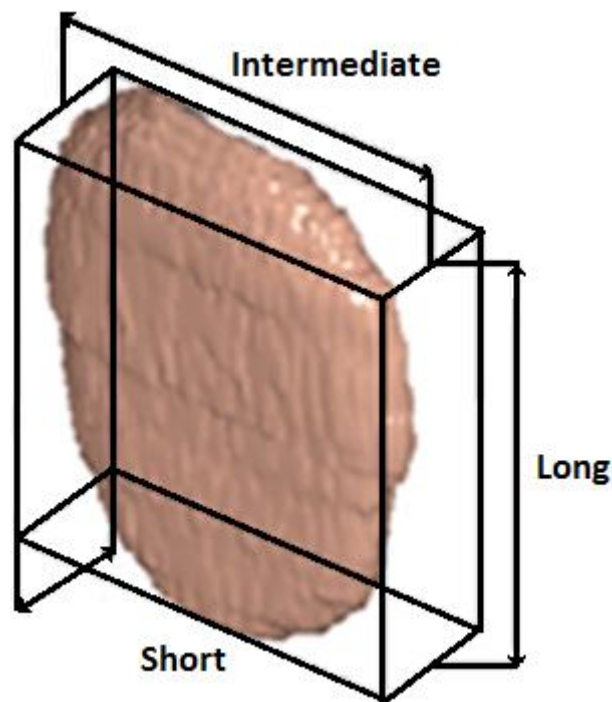


Figure 2.9 Principal dimensions of an aggregate.

$$Sphericity = \sqrt[3]{\frac{S * I}{L^2}} \quad (2.3)$$

According to Wadell, (1935), sphericity is defined as “ratio of particle with sphere diameter of equivalent volume and smallest sphere diameter that is surrounding of particle”. Krumbein, (1991) developed the definition that is based on the dimensions regarding three different axis instead of smallest sphere diameter surrounding the particle.

Form is also defined by “shape factor” and is used to discriminate particles from each other (Hudson, 1999), (Mora & Kwan, 2000). According to Aschenbremer (1956) shape factor is defined by a relationship between the main size of particle (long, intermediate, short) (Equation 2.4). According to this equation, if increasing sphericity value greater than 1, it is long and if decreasing sphericity value less than 1, it is flat.

$$\text{Shape Factor} = \frac{S}{\sqrt{L * I}} \quad (2.4)$$

Besides sphericity and shape factor definitions, two measures are also defined as “Elongation” or “Length factor” (Equation 2.5) and “Flatness factor” (Equation 2.6) in order to get better description of aggregate shape (Aschenbrenner, 1956), (Kuo, Rollings, & Lynch, 1998).

$$\text{Elongation} = \frac{L}{S} \quad (2.5)$$

$$\text{Flatness} = \frac{S}{I} \quad (2.6)$$

Other definitions about aggregate characteristics are:

- Aspect Ratio
- Rugosity

- Radius Ratio
- % Rectangle Area
- Convexity
- Roundness

2.2.1.1 Aspect Ratio (R_c)

The ratio of the major to minor axes of an ellipse that has the same first moment as the particle outlines (Figure 2.10) (Persson, 1998).

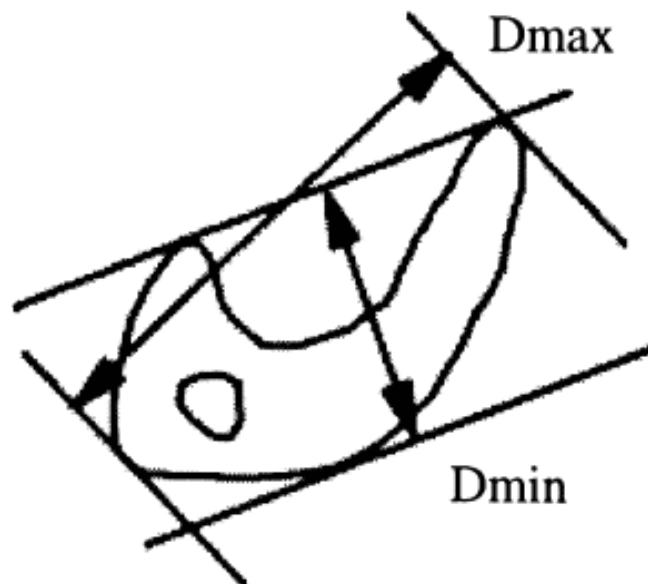


Figure 2.10 The aspect ratio of the object (Persson, 1998).

$$\text{Aspect Ratio} = \frac{D_{min}}{D_{max}} \quad (2.7)$$

2.2.1.2 Rugosity (R_g)

Dilek, (2000), deduced rugosity property that is related to the ratio of the perimeter of the particle (P) to the perimeter of a rectangle, which encloses the particle (Figure 2.11).

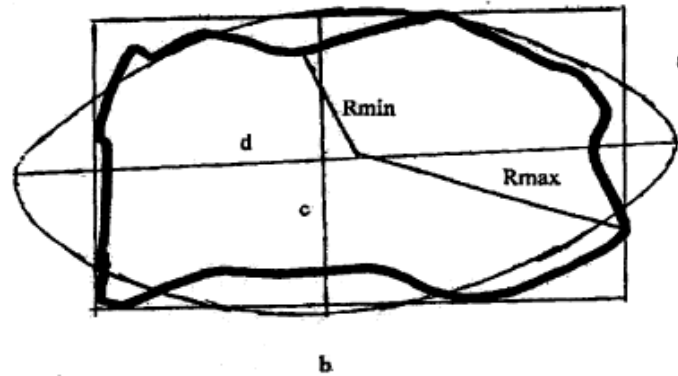


Figure 2.11 Angularity measures (Dilek, 2000).

$$R_g = \frac{P}{2(a + b)} \quad (2.8)$$

Where P : perimeter of aggregate

a : short side of rectangle that encloses the particle

b : long side of rectangle that encloses the particle

2.2.1.3 Radius Ratio (R_y)

Radius Ratio is the ratio of the maximum radius to the minimum radius that is the maximum and minimum possible distances respectively from the centroid of the particle to its perimeter (Figure 2.11). A highly irregular surface is likely to have a very small minimum radius and radius ratio will increase (Dilek, 2000).

$$R_y = \frac{R_{max}}{R_{min}} \quad (2.9)$$

2.2.1.4 % Rectangle Area (%DA)

Rectangle Area is the ratio of the particle area to the area of the rectangle enclosing the particle (Dilek, 2000).

$$\%DA = \frac{A}{a * b} \quad (2.10)$$

2.2.1.5 Convexity (C)

Convexity (Mora & Kwan, 2000) can be evaluated by means of the convexity ratio C that is defined as:

$$C = \frac{A}{CA} \quad (2.11)$$

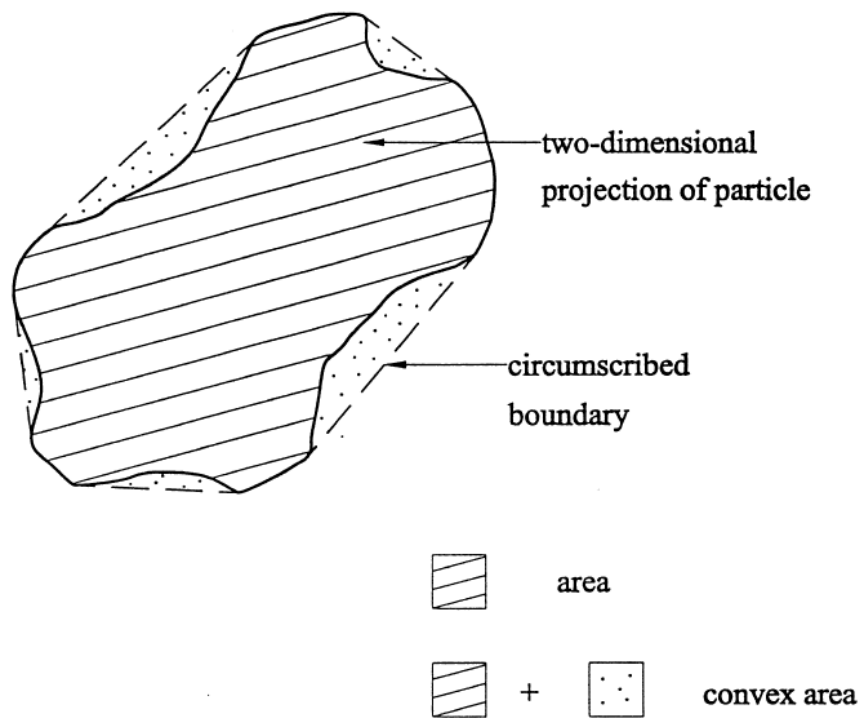





Figure 2.12 Convexity of aggregate (Mora & Kwan, 2000).

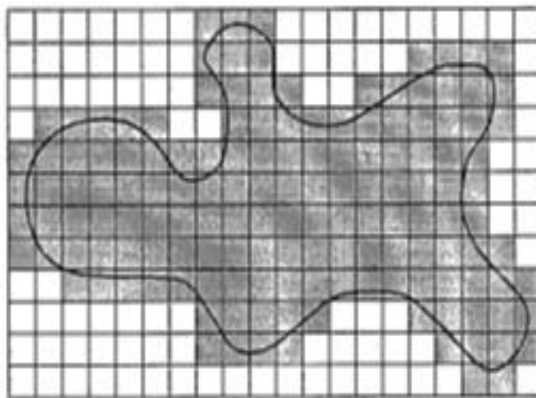
Where:

- A (Area) = 
- CA (Convex Area) =  + 

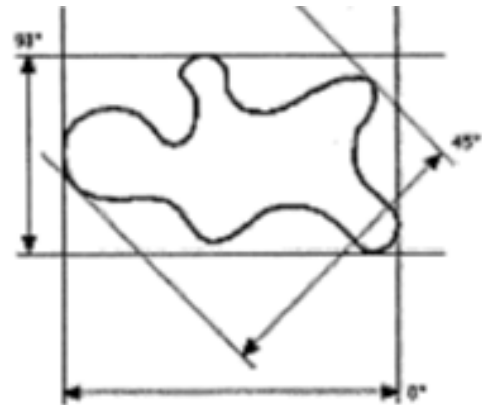
2.2.1.6 Roundness

Roundness (Janoo, 1998) is a common measure computed from two-dimensional image of aggregate particle as shown in Figure 2.13 and described as:

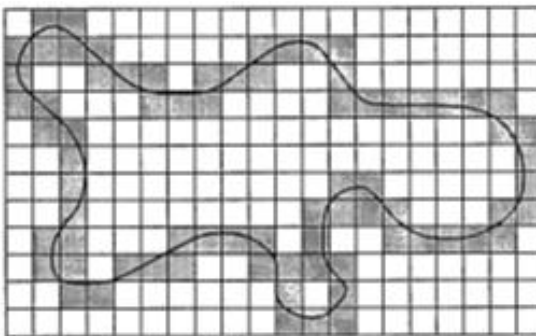
$$\text{Roundness} = \frac{P^2}{4\pi A} \quad (2.12)$$



a. Area of an aggregate calculated through image analysis.



c. Typical ferret measurement.



b. Perimeter of an aggregate calculated through image analysis.



d. Illustration of convex perimeter.

Figure 2.13 Material characterization using image analysis (Janoo, 1998).

Where P and A are perimeter and area of object, and, if roundness value is 1, the object is circular (Al-Rousan, 2004).

A commonly used scale for describing aggregates in the USA is given as follows (Mora, Kwan, & Chan, 1998):

- Angular: Little evidence of wear
- Sub-angular: Some wear but faces untouched
- Sub-rounded: Considerable wear, faces reduced in area
- Rounded: Faces almost gone
- Well-rounded: No original faces left

We can see shape definitions comparatively in Figure 2.14.

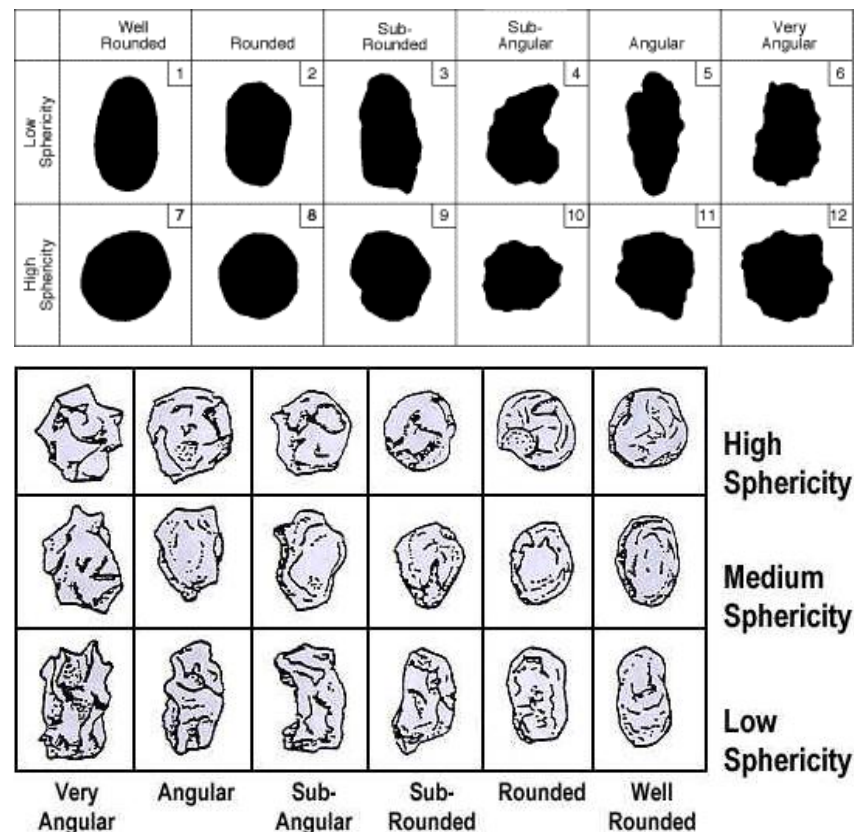


Figure 2.14 Aggregate roundness and angularity scale (MacLeod, 2002), (Krumbein & Sloss, 1951).

2.2.2 Aggregate Texture

The surface texture, also called surface roughness, is the local corrugations of the surface of ideal flat shape (Figure 2.15). Surface texture of the aggregate may be rough or smooth and plays an important role for the formation of bonds between aggregate and pasting material in production process of the concrete or asphalt. Surface texture provides a gripping structure producing stronger bonds, and resulting stronger asphalt or concrete (Janoo, 1998), (Anonymous, INDOT, 2011). In the literature, (Bikerman, 1964), (Terzaghi & Peck, 1967), (Wright, 1955), (Barksdale & Itani, 1994), (Masad, 2002) defined surface texture of aggregates and used different methods to measure them.

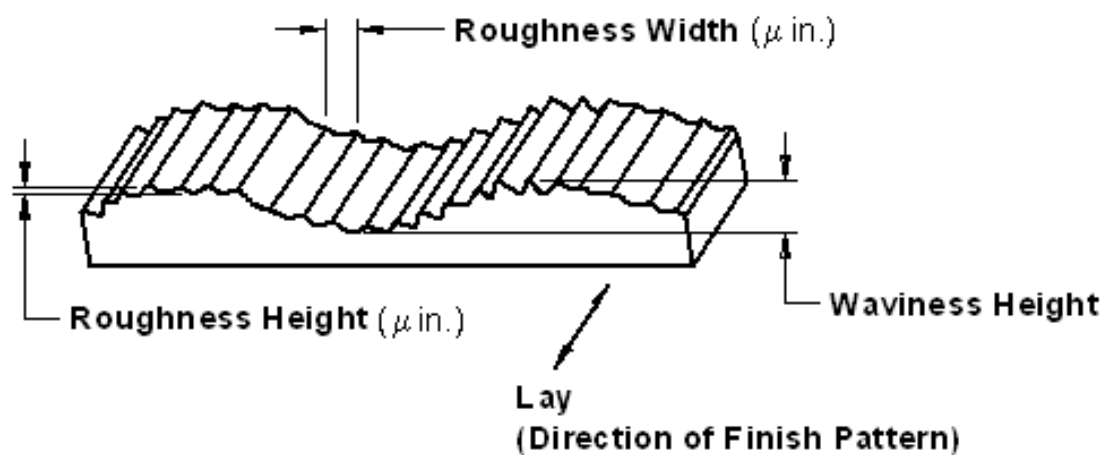


Figure 2.15 Surface texture (roughness) of a material (Anonymous, Surface Roughness Review, 2011).

2.2.3 Aggregate Size and Shape Measurement by Using Digital Image Processing

Sieving method is commonly used for measuring aggregate size. However, it has many disadvantages such as; being time consuming, high cost, too inefficient, prone to human errors, being just a bulk approximation, etc. For decades, advances of

computer technologies together with digital image processing techniques have become increasingly prevalent for many applications.

Analyzing aggregate by using digital image processing (DIP) techniques has been extensively used for the past 20 years. Compared with traditional methods, it is found that DIP techniques have many advantages such as; low cost, high performance, more automated, being simple to implement, etc. From this point of view, 3D image processing techniques are given in the following chapter.

CHAPTER THREE

3D IMAGE PROCESSING

3.1 Introduction

Many kind of animals receive the information about their surroundings without depending on their eyes, such as; bats use high-frequency sound, cats have a rich sense of smell and hearing ability, snakes locate prey by their heat emission, sharks have organs that sense electrical fields (Gonzalez & Woods, 2002), (Russ, 2002), (McAndrew, 2004). However, human beings perceive, process, analyze and classify visually and they have the ability of seeing all the objects around them in 3D. Researchers are still studying on human vision (Jain, Kasturi, & Schmoh, 1995).

Aims of computer vision are to perceive and understand an image on the scene electronically like human vision. Advanced charge coupled devices (CCD) and digital image processing methods have been utilized in widespread applications (manufacture, security field, geographical information systems, etc.) for the past years. Digital image processing is a basic field of computer vision because it is used in the process of creating a model of the real world from images (Jähne, Haussecker, & Geissler, 1999), (Ferron, 2000), (Gonzalez & Woods, 2002).

Digitized images give us 2D information, but it is not enough for the real world because we live in a 3D world. When capturing images of an object in 3D space, the image sensors give two-dimensional projections, and this cause many information loss and decreases number of dimensions.

A 3D image has many advantages over its 2D counterpart, which are;

- 3D images express the geometry in terms of 3D coordinates,
- Volume of an object is calculated from its 3D data,
- 3D images can give surface texture,

- Size, position and shape of an object in a scene can be straightforwardly computed from its 3D coordinates.

In many cases, image-based methods are the only way for measurements, but as a manual visual interpretation and calculation, requirements may be difficult. 3D imaging can most of the times minimize the requirements for visual inspection. This is an advantage in terms of time and cost.

3.2 3D Imaging-Related Issues

Summaries of some important 3D imaging related topics are given in this part. These topics are digital image processing, computer graphics, computer vision, and pattern recognition. Reader can find further and detailed information in the references given.

3.2.1 Digital Image Processing (DIP)

The smallest element of a digital image in the spatial coordinate plane is pixel. A digital image is formed by more than one pixel with the gray levels or intensity (Figure 3.1). Digital image processing extracts information for human interpretation or edits information for automatic perception into a digital image. DIP is a technique that has different algorithms, such as; blurring, cropping, resizing, enhancement, etc., for images in 2D data (Jähne B. , 2002), (Pratt, 2001), (Russ, 2002), (Young, Gerbrands, & Vliet, 1995).

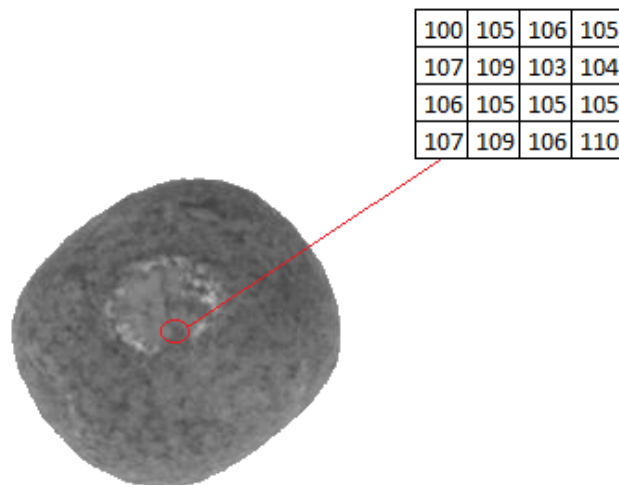


Figure 3.1 Gray levels of an aggregate image.

3.2.2 Computer Graphics (CG)

Computer graphics renders objects to look like to its real life counterpart with "realistic" study. One major factor holding back low-end computer graphics is created patterns appear too smooth (Figure 3.2). In addition, natural objects have surface texture (Shapiro & C., 2001), (Çetin & Güdükbay, 2006).



Figure 3.2 A modern render of the Utah teapot, an iconic model in 3D computer graphics created by Martin Newell in 1975.

3.2.3 Computer Vision (CV)

Computer vision gathers information for perception the objects on the environment through using optical devices without any physical interaction. As shown Figure 3.3, CV contains image processing techniques, pattern recognition, artificial intelligence and different kinds of classifiers (Forsyth & Ponce, 2002), (Jain, Kasturi, & Schmoh, 1995), (Shirai, 1992).

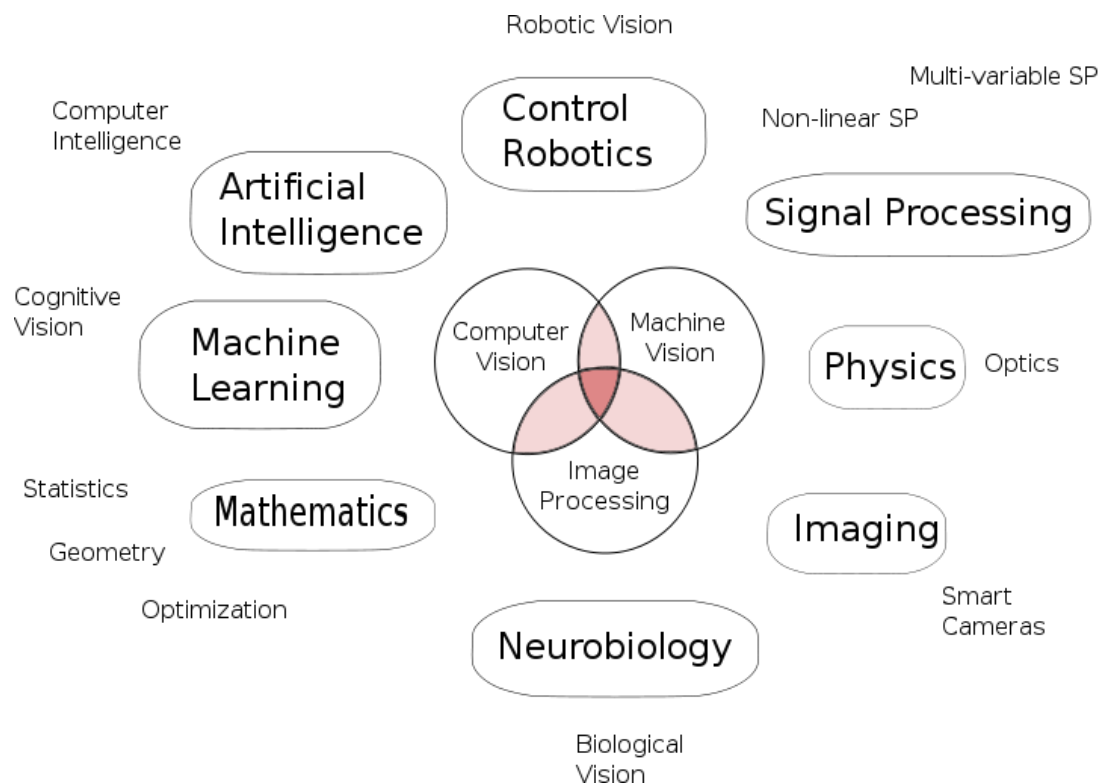
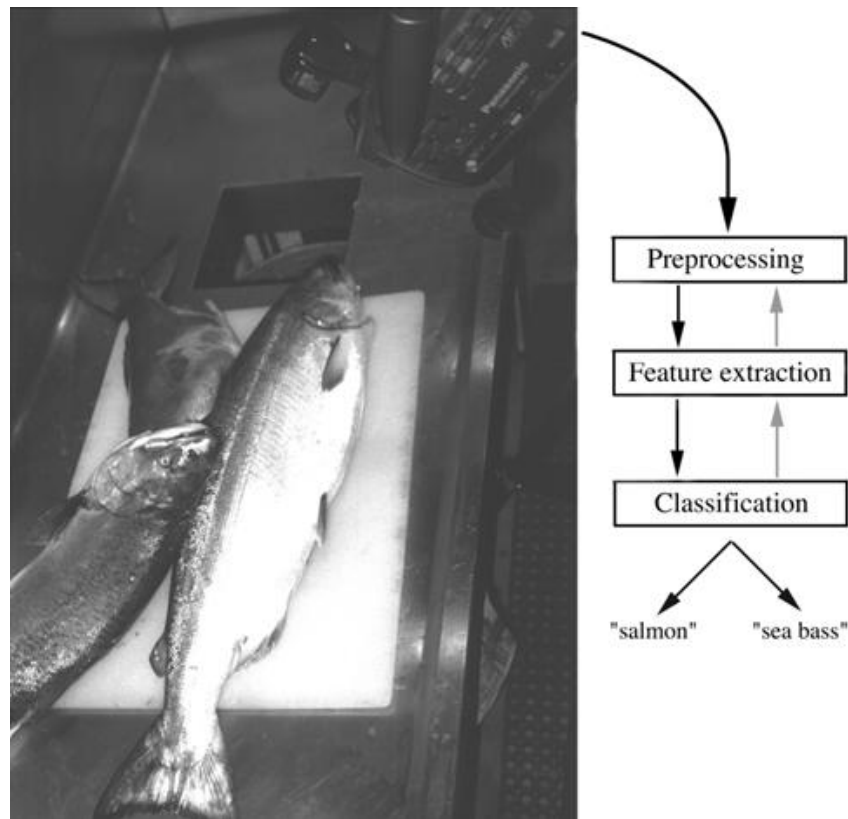


Figure 3.3 Relation between computer vision and various other fields (Anonymous, Computer Vision, 2011).

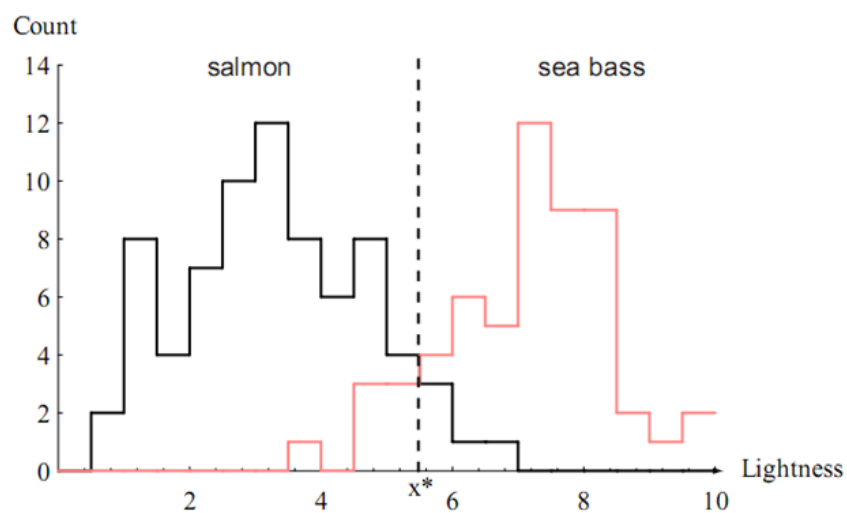
3.2.4 Pattern Recognition (PR)

Pattern recognition algorithms classify numeric or symbolic data through using the feature vectors (patterns) according to different types of learning or training procedures. It aims to make decisions about patterns. It has many application fields like handwritten character recognition, biometrics, speech recognition, medical

diagnosis, etc. (Bishop, 2006), (Duda, Hart, & Stork, 2000), (Sá, 2001). As simple example is given from the book of Duda, Hart & Stork in Figure 3.4.



(a) Example of classification



(b) Histograms of values

Figure 3.4 An example of pattern recognition (Duda, Hart, & Stork, 2000).

3.3 3D Data Acquisition

3D data can be acquired through recent technological advances related with CCD cameras, computers and laser sources. 3D data acquisition allows the generation of 3D models using different methods and systems. In this section, different 3D data acquisition systems are explained.

3.3.1 Laser Ranging System

Laser ranging systems are based on distance measurement to an object using laser beam. It measures time of the laser pulse sent and reflected from the object's surface (Marshall D., 1997). Laser ranging systems are used in different application areas, such as; military, forest, sports, industrial, etc.

3.3.2 Structural Light Method

A grid or a stripe light pattern is sent on the object and the deformation of the pattern reflected from surface of the object is captured using a digital camera. The model of the object is extracted through measuring the distance at each point in the deformed pattern (Figure 3.5). The most important property of the method is its simplicity and its speed (because of scanning multiple points), but it has low spatial resolution (Figure 3.6) (Anonymous, 3D scanner, 2011).

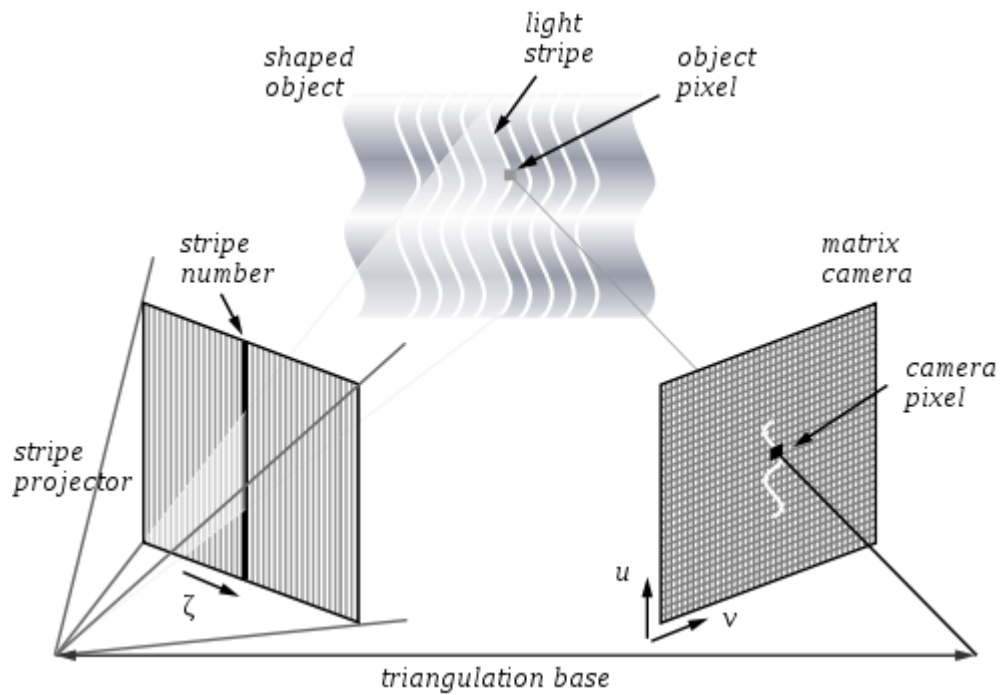


Figure 3.5 Triangulation principle shown by one of multiple stripes (Anonymous, Structured-light 3D scanner, 2011).

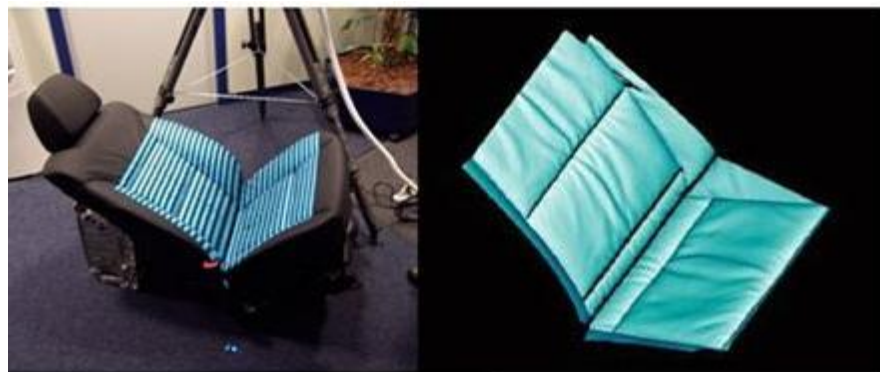


Figure 3.6 3D survey of a car seat (GFMesstechnik, 2008).

3.3.3 Moirè Fringe Method

Property of this method is that the sent light is distributed by a grid then it is reflected from the surface of the object, which is shown in Figure 3.7 (a). Thus, the image is formed by mixing the reference and Moirè fringe patterns that has the dark

and light lines (Figure 3.7 (b)). Change in the depth and shape are detected by analysis of this pattern (Creath & Wyant, 2008).

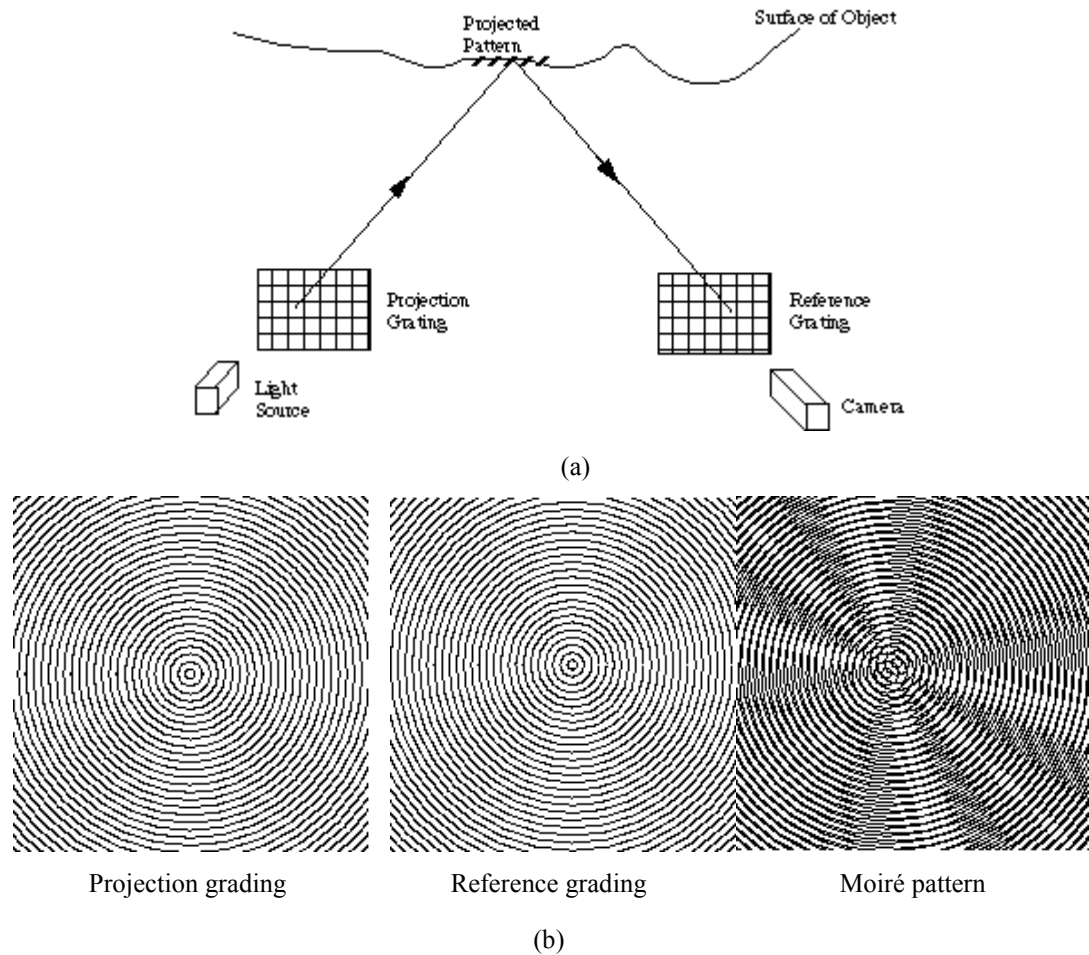


Figure 3.7 Moiré systems (Marshall D., 1997).

3.3.4 Shape from Shading Method

This method uses the photometric stereo techniques to measure depth. The object is illuminated with different light sources positioned around it. Images of the object (which is fixed in position) are taken using one or more cameras during this illumination time. This technique is not very suitable for 3D data acquisition, because it is very sensitive to lighting conditions and reflection property of the object (Jähne B., 2002), (Trucco & Verri, 1998).

3.3.5 Passive Stereoscopic Method

The aim of the stereoscopy is to create a 3D depth model from two images of a scene using two cameras. Cameras are separated by a specific distance in the same plane. 3D depth map of object is reconstructed using paired similar features of images (Anonymous, Stereoscopy, 2011). Main problem of this method is matching (registration) process that is very difficult to find similar features of two images.

3.3.6 Active Stereoscopic Method

Active stereoscopic method contains a camera and a strong light source instead of two cameras. The scene is illuminated with the light source that is observed with the camera. Depth map is constructed for the whole of the scene scanned by the light source (Marshall D., 1997), (Dipanda A., Woo, Marzani, & Bilbault, 2003).

3.4 3D Imaging Techniques

3D imaging indicates an image of an object in all three real world dimensions. In Cartesian coordinate system, these dimensions correspond to object's length, width and height. The aim of this section is to provide an overview of different 3D imaging techniques.

3.4.1 Time-of-Flight (ToF) Technique

In this technique, the laser light is used for gathering data on the object. The laser light is sent from the source to the object and reflected light returns to the receiver. The time of sent-received signal is measured. The distance is calculated as in Equation 3.1 (Jähne B., 2002), (Schwarte, Häusler, & Malz, 2000).

$$d = \frac{c * t}{2} \tag{3.1}$$

Where d : distance,

c : the speed of light,

t : time.

The speed of light (c) is $3 \cdot 10^8 \text{ ms}^{-1}$ in ideal conditions, and the time (t) is measured from sent-received signal. Thus, the distance (d) is simply calculated.

Nowadays, this method is used in different applications such as; face gesture detection and measurement of human body height (Dorrington, Kelly, McClure, Payne, & Cree, 2009), (Meers & Ward, 2009).

3.4.2 Triangulation Technique

In this technique, laser light source is used to illuminate a point on an object of interest. Captured image contains reflected laser dot and this dot moves on the image with an amount directly related with the distance between object and the camera. This technique is called as triangulation. In this technique, angles and distance of the laser light and the detector are known, thus, X - Y - Z values of a surface point on the object are calculated using simple trigonometry in the X - Y - Z coordinate's plane. Triangulation has four principal categories; stereoscopy, active triangulation, focus and confocal microscopy (Anonymous, 3D scanner, 2011), (Russ, 2002), (Beato, 2011), (Grossmann, 1987), (Shim & Choi, 2010), (Kovács, 2004), (Price, Fundamentals: Three-dimensional Imaging, 1996), (Jähne B. , 2002), (Semwogerere & Weeks, 2005), (Al-Awadhi, Hurn, & Jennison, 2011).

3.4.3 Interferometry Technique

Interferometry is similar to time-of-flight technique. Although ToF measures sent-reflected signal time, interferometry measures amplitude and phase of the signal that is interfered with a reference signal (Jähne, 2002). (Anonymous, Interferometry, 2011).

3.5 Dynamic 3D-Vision

Photonic Mixer Device (PMD), which is developed by PMDTechnologies[®], is a new generation of time-of-flight camera. ToF technique is explained in Section 3.4.1. ToF cameras use a single laser beam, PMD devices use integrated 64 x 48 smart pixel array to send and receive multiple laser beams (Schwarte R., 2001), (Ringbeck & Hagebeuker, 2007).

In this chapter, we discussed the importance of some 3D data related issues because it is directly related with real world objects. Different 3D imaging techniques and data acquisition methods are explained. Some studies in the literature are also addressed. 3D imaging and analysis system is developed after reviewing all the methods that are mentioned in this chapter. Detailed information about developed 3D imaging and analysis system for aggregates is given in the following chapter.

CHAPTER FOUR

MATERIAL AND METHODS

4.1 Introduction

In this chapter, developed 3D imaging system for the analysis of the aggregates (image acquisition, feature extraction and classification) is explained. In addition, 2D image analysis techniques and manual methods are given. They are compared with developed 3D analysis system to depict the advantages of the 3D system. Six¹ different types of aggregates are used for the analysis and comparison process, which are explained in the following section.

4.2 Material

Natural aggregate can be acquired in two ways: By crushing big rocks into smaller pieces and by excavating aggregate reach fields that are formed during time. Sieving, crashing and washing processes can be applied to these types of aggregates. In this study, six different types of Dalaman natural aggregate are used. An expert manually classified these samples and labeled each of them as angular, flat, round, formless, sphere and elongate (Figure 4.1). Total values of labeled aggregates are given Table 4.1. All aggregate samples are (Dalaman natural aggregate) provided by Famerit Company.

¹ Sphere type aggregate are actually a ball shaped metal objects that are used in cement production. Experts from Dokuz Eylül University Civil Engineering Department used (for concrete production) and named these objects as aggregate. The experts approved usage of these as sixth type of aggregate.

Table 4.1 The number of samples for different shaped aggregate types.

No	Class	Total Count	Total Weight (Kg)
1	Elongate	228	0,675
2	Flat	447	0,705
3	Angular	297	1,665
4	Sphere	435	5,625
5	Round	519	1,155
6	Formless	267	1,260



Figure 4.1 Sample images showing different aggregate types (a) Elongate, (b) Sphere, (c) Angular, (d) Round, (e) Irregular, (f) Flat.

4.3 Method

In this section, methods which are used in this thesis work are given in detail. Graph paper is used in manual measurement method. L, S and I values are measured sensitively and recorded. 2D image analysis part contains imaging, preprocessing

and feature extraction works. 3D image analysis section explains all the accomplishment achieved during 3D imaging system development and gives detailed information related with 3D reconstruction and feature extraction works.

4.3.1 Manual Measurement Method

The aim of the manual measurement is to acquire the real size of the aggregate for comparison with the developed 3D imaging system. Six samples from each of six different aggregate classes (as shown Figure 4.2 (a-f)) are randomly selected for measuring the L, S and I values.

Graph paper is used for the manual measurement method. The top and side projections on the graph paper are measured and L, S and I values for each of the aggregates are recorded. Results are shown in Table 4.2.



a) Formless type aggregates (top and side views).



b) Roundness type aggregates (top and side views).



c) Sphere type aggregates (top and side views).



d) Angularity type aggregates (top and side views).



e) Flat type aggregates (top and side views).



f) Elongate type aggregates (top and side views).

Figure 4.2 L, S and I measurement of aggregate samples with top and side views.

Table 4.2 Manual measurement result.

No	Class	L (cm)	S (cm)	I (cm)
1	Elongate	2.8	1.8	0.9
2	Elongate	1.8	0.9	0.9
3	Elongate	1.8	0.9	0.9
4	Elongate	2.1	1.2	0.6
5	Elongate	3.0	1.9	0.9
6	Elongate	3.8	1.6	1.1
7	Flat	2.8	2.3	0.9
8	Flat	2.3	2.5	0.9
9	Flat	2.3	1.9	0.5
10	Flat	1.6	2.1	0.6
11	Flat	2.0	1.8	0.6
12	Flat	1.3	1.3	0.6
13	Angular	2.2	2.1	1.9
14	Angular	3.8	1.9	2.1
15	Angular	2.8	2.0	1.8
16	Angular	2.0	1.8	1.1
17	Angular	3.1	1.4	1.8
18	Angular	2.3	1.6	1.3
19	Sphere	2.7	2.5	2.3
20	Sphere	2.2	2.6	2.0
21	Sphere	1.8	1.7	1.4
22	Sphere	1.8	2.0	1.5
23	Sphere	1.6	2.1	2.0
24	Sphere	1.4	1.4	1.0
25	Round	1.8	1.5	1.1
26	Round	1.8	1.5	0.6
27	Round	1.3	1.3	0.6
28	Round	1.5	1.2	0.9
29	Round	1.4	1.1	0.9
30	Round	1.2	1.0	1.0
31	Formless	2.0	1.4	1.2
32	Formless	1.5	1.1	0.9
33	Formless	1.3	1.4	1.0
34	Formless	2.5	2.1	1.8
35	Formless	2.0	1.5	1.2
36	Formless	2.4	1.3	1.9

4.3.2 Two-Dimensional Method

In this section, 2D imaging system, preprocessing and feature extraction methods are explained for measuring aggregate dimensions. The purpose of the work given in this section is to obtain L, S and I values of aggregates using 2D image analysis method. As a result, advantages of the developed 3D image analysis system can be demonstrated in a comparative way. Flow chart of the 2D image processing method is shown in Figure 4.3.

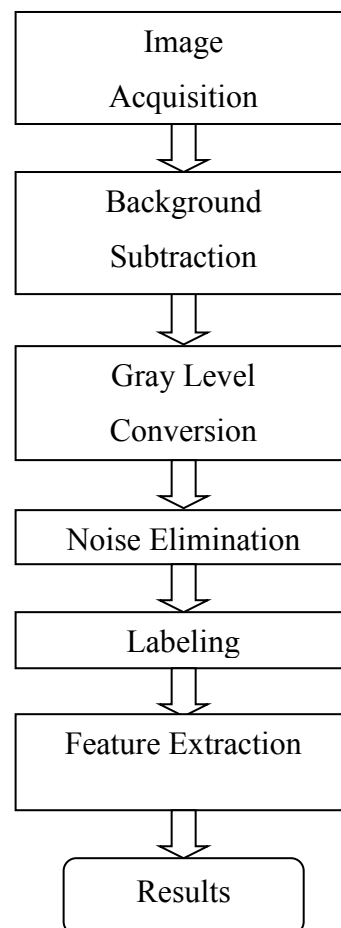


Figure 4.3 Flow chart of the 2D image processing method

4.3.2.1 Imaging System

Imaging system is set on medium density fiberboard coated panel, which is 50 cm x 50 cm in size, surrounded by white fabric in order to make a homogeneous lighting. 2 x 9 W halogen lamps and 1 x 24 W fluorescent lighting diffuser are used for a homogeneous illumination. To prevent the reflection, the base is covered with a white and matte paperboard. Sony[®] DSC-R1 digital camera, which is placed on a tripod to prevent vibrations that may occur during shooting is used to capture images (Figure 4.4). The top and side view images of aggregates (Figure 4.5) are taken separately to find their L, S and I values. Images are stored one by one as JPG file type in 3888 x 2592 image sizes as top and side views.



Figure 4.4 2D imaging system setup

4.3.2.2 Preprocessing

The images are preprocessed with 2D image processing techniques. Firstly, captured images are combined and converted to gray scale image as shown in Figure 4.6. All artifacts containing less than 30 pixels are removed from the image (Figure 4.7). Thirdly, edges are detected using canny edge algorithm. After that, holes (that can occur as a background section inside of the aggregate image region) are filled in the image and aggregates are labeled. Figure 4.8 shows color coded form of the labeled image. Lastly, long, intermediate and short values are measured using bounding box method (Figure 4.9).



Figure 4.5 2D top and side views of aggregates.

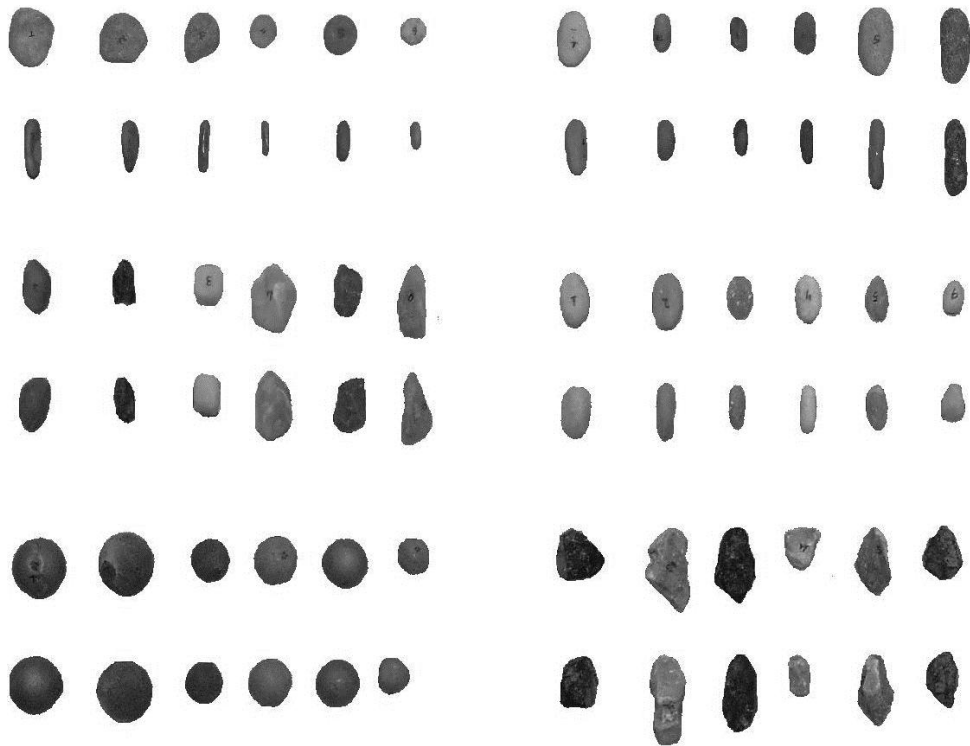


Figure 4.6 Gray scale images of aggregate samples.

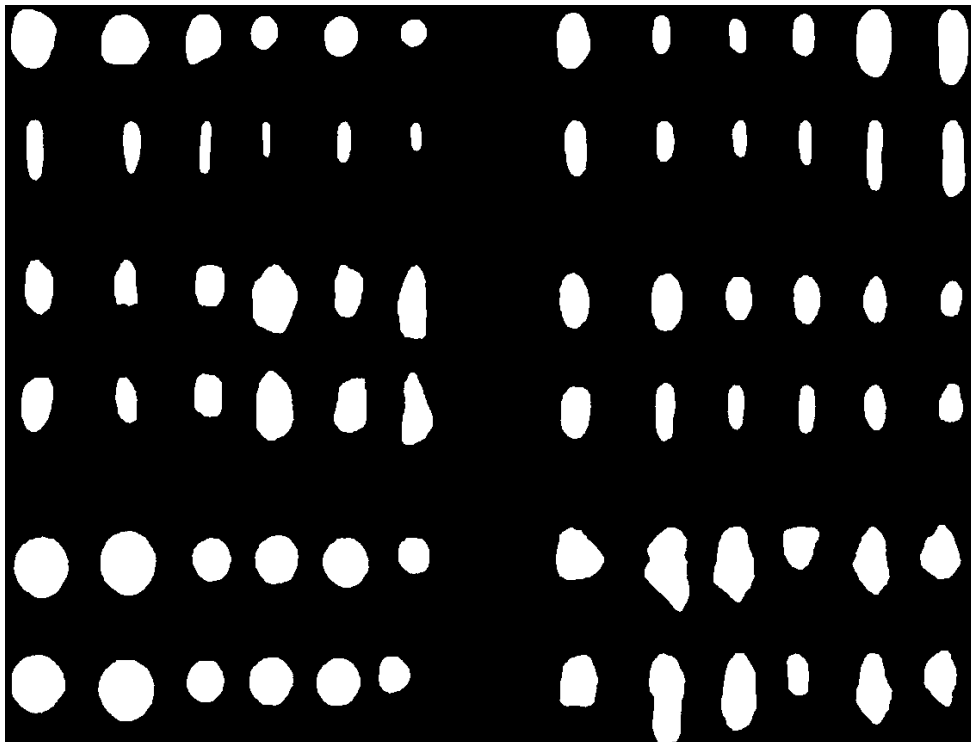


Figure 4.7 Removing all objects than 30 pixels.

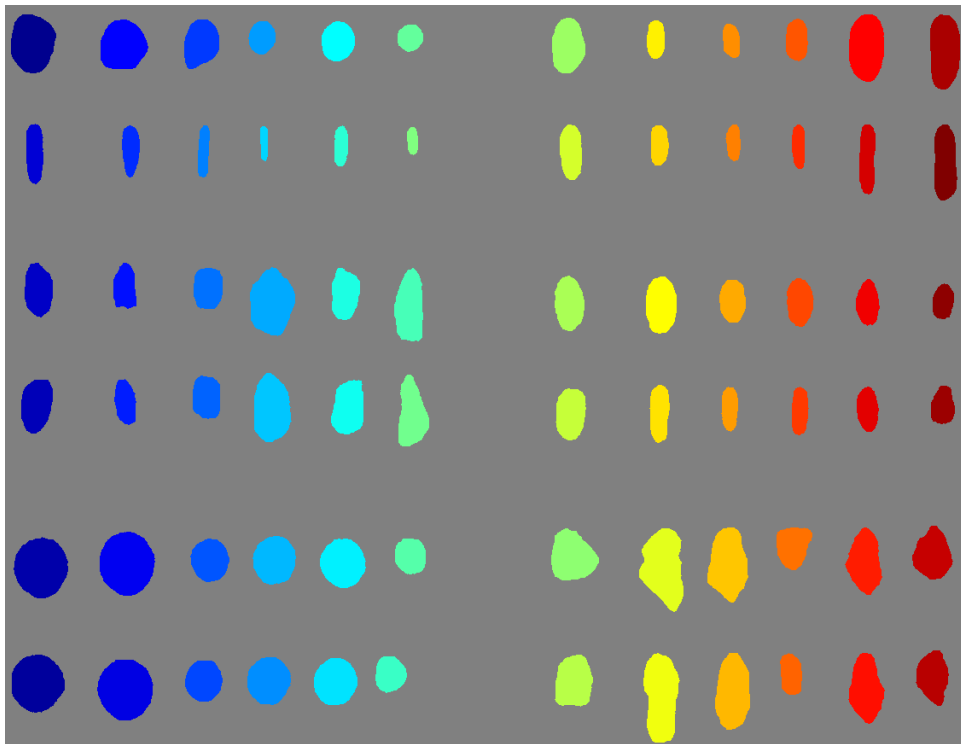


Figure 4.8 Color labeling of aggregates.

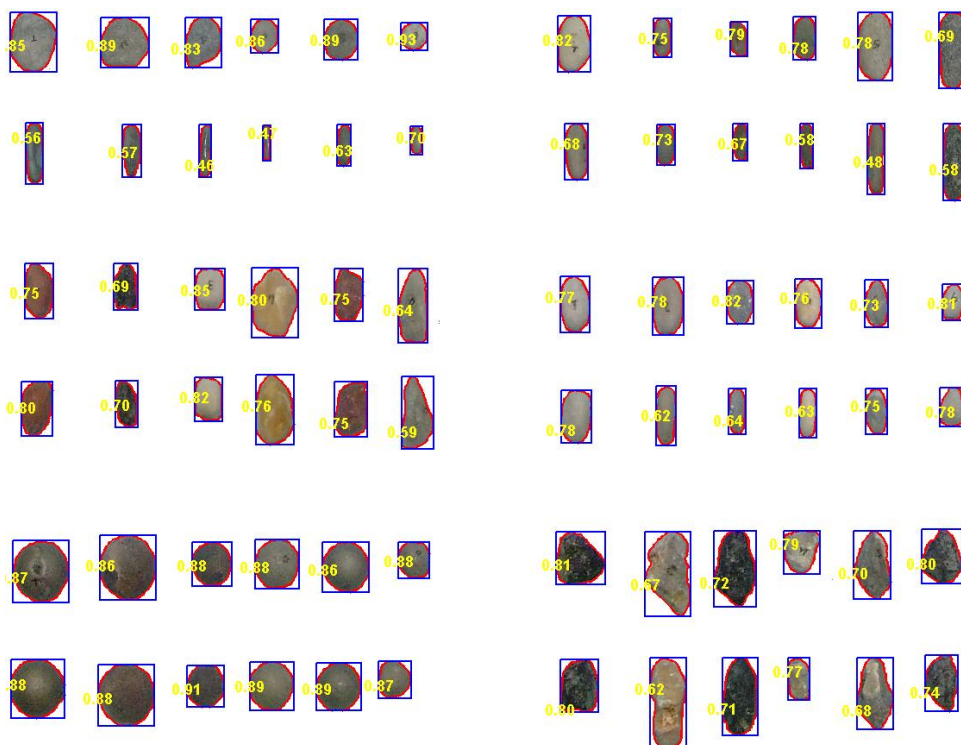


Figure 4.9 Measuring the L, S and I values.

4.3.2.3 Feature Extraction

The L, S and I values are measured from segmented images of aggregate are shown in Figure 4.2 (a-f). Resolution of capturing images is 300 pixels/inch, so, the L, S and I values are converted from pixel to centimeter using Equation 4.1. These values are used to calculate sphericity, shape factor, elongation and flatness factor (Equation 1.1 – 1.4). This process is repeated for six different samples of six aggregate types. The measurement results are shown in Table 4.3.

Table 4.3 Measurement results of 2D top and side views images of aggregate.

No	Class	L(cm)	S(cm)	I(cm)	Sphericity	Shape Factor	Elongation	Flatness
1	Elongate	2,8	1,8	1,1	0,61787	1,00240	1,61589	1,62366
2	Elongate	2,1	1,0	0,9	0,59439	0,69567	2,14286	1,03704
3	Elongate	1,9	1,0	0,8	0,58538	0,80390	1,97590	1,27692
4	Elongate	2,2	1,2	0,8	0,56435	0,91961	1,87379	1,58462
5	Elongate	3,5	1,9	0,9	0,50968	1,05921	1,88820	2,11842
6	Elongate	3,9	1,6	1,3	0,51653	0,72903	2,39007	1,27027
7	Flat	3,0	2,4	1,1	0,66171	1,30217	1,26733	2,14894
8	Flat	2,6	2,5	0,7	0,63994	1,75057	1,07583	3,29688
9	Flat	2,5	1,8	0,6	0,55231	1,48897	1,38854	3,07843
10	Flat	1,7	1,4	0,4	0,59305	1,57079	1,24786	3,07895
11	Flat	2,0	1,7	0,7	0,68832	1,42429	1,14765	2,32813
12	Flat	1,3	1,3	0,5	0,73560	1,52342	1,02679	2,38298
13	Angular	2,3	2,0	1,6	0,85162	1,02001	1,15882	1,20567
14	Angular	3,6	1,9	1,7	0,63206	0,76991	1,88344	1,11644
15	Angular	3,2	2,0	1,5	0,66360	0,89911	1,61765	1,30769
16	Angular	1,7	1,5	0,9	0,78014	1,19472	1,13846	1,62500
17	Angular	3,0	1,5	1,5	0,62832	0,70989	2,00000	1,00787
18	Angular	2,3	1,9	1,5	0,80174	1,01961	1,23125	1,28000
19	Sphere	2,5	2,4	2,4	0,99208	0,99764	1,00957	1,00481
20	Sphere	2,5	2,5	2,5	0,98927	0,99541	1,01395	1,00467
21	Sphere	2,0	1,9	1,7	0,94784	1,03649	1,03012	1,10667
22	Sphere	2,0	2,0	2,0	0,98288	0,99146	1,02326	1,00585
23	Sphere	2,0	1,7	1,7	0,91737	0,95168	1,12667	1,02041
24	Sphere	1,5	1,5	1,4	0,97560	1,03775	1,00000	1,07692
25	Round	1,9	1,5	1,2	0,77794	1,00098	1,28462	1,28713
26	Round	2,1	1,5	0,8	0,64776	1,22132	1,35115	2,01539

No	Class	L(cm)	S(cm)	I(cm)	Sphericity	Shape Factor	Elongation	Flatness
27	Round	1,5	1,3	0,7	0,72906	1,26743	1,17117	1,88136
28	Round	1,7	1,2	0,7	0,67094	1,15699	1,35238	1,81035
29	Round	1,6	1,1	0,9	0,74578	0,97111	1,36735	1,28947
30	Round	1,2	1,0	1,0	0,86297	0,92753	1,21839	1,04819
31	Formless	2,1	1,5	1,3	0,77045	0,88067	1,41270	1,09565
32	Formless	1,7	1,1	1,1	0,77026	0,83515	1,46392	1,02105
33	Formless	1,5	1,4	1,2	0,90842	1,06296	1,05691	1,19418
34	Formless	2,5	2,2	1,6	0,83124	1,10486	1,12566	1,37410
35	Formless	2,1	1,6	1,3	0,78209	0,96500	1,30935	1,21930
36	Formless	2,7	1,5	1,3	0,64753	0,78327	1,81746	1,11504

Average of feature vectors values are calculated. The results are shown in Table 4.4. Elongation value of elongate type aggregate is greater than the other aggregate types, though sphere type aggregate has smallest elongation value. Sphere type aggregate has maximum value of sphericity, and flat type aggregate has maximum flatness and shape factor values. This shows that the feature vectors of sphericity, elongation, shape factor and flatness can be used for discriminating these types of aggregates. However, angular, formless and round types of aggregates are not successfully classified because of inappropriate features.

Table 4.4 Average of feature vectors values.

No	Class	Sphericity	Shape Factor	Elongation	Flatness
1	Elongate	0,56470	0,86830	1,98112	1,48516
2	Flat	0,64516	1,51004	1,19233	2,71905
3	Angular	0,72625	0,93554	1,50494	1,25711
4	Sphere	0,96751	1,00174	1,03393	1,03656
5	Round	0,73908	1,09089	1,29084	1,55532
6	Formless	0,78499	0,93865	1,36433	1,16989

4.3.3 Three-Dimensional Method

Firstly, imaging system (as hardware and software) is designed. Sample aggregates' images are captured by using this system. Secondly, stored images are

preprocessed using image processing techniques for segmentation, and segmented images are reconstructed to form a 3D image of the aggregate. Thirdly, feature vectors are extracted from reconstructed images of aggregates. 3D image analysis system is shown in Figure 4.10. Classification work using feature vectors of aggregates is given in Section 4.4 of this chapter.

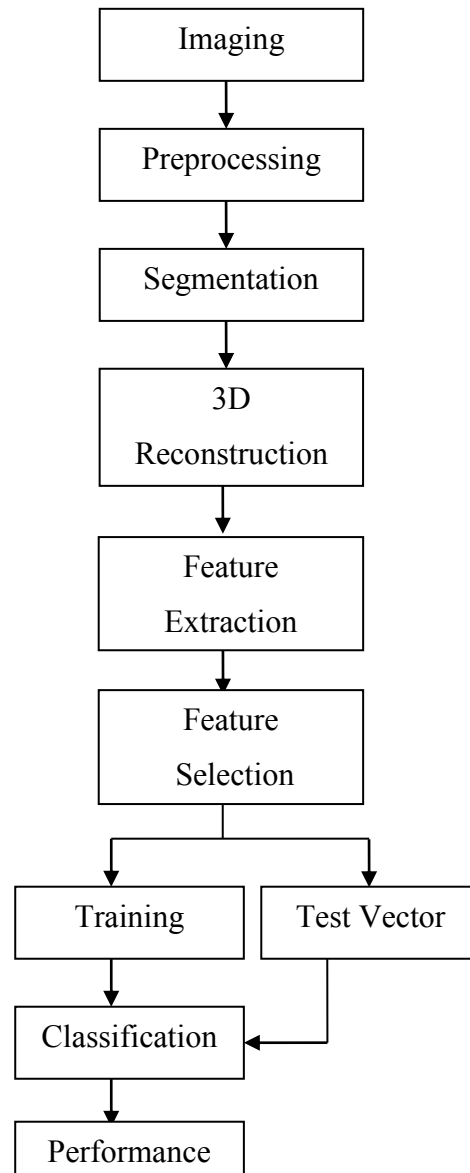


Figure 4.10 Flow diagram of three-dimensional image analysis system.

4.3.3.1 Imaging System

3D imaging system is created and used to acquire images of different classes of the aggregates. The aim of this system is to capture laser projections that are created at a certain distance on the aggregate by the laser source. Two cameras that have the same characteristics are placed symmetrically on opposite sides on the laser source. A step motor is used to move the conveyor belt so that all upper side of an aggregate can be scanned. An illustration of the system is shown in Figure 4.11.

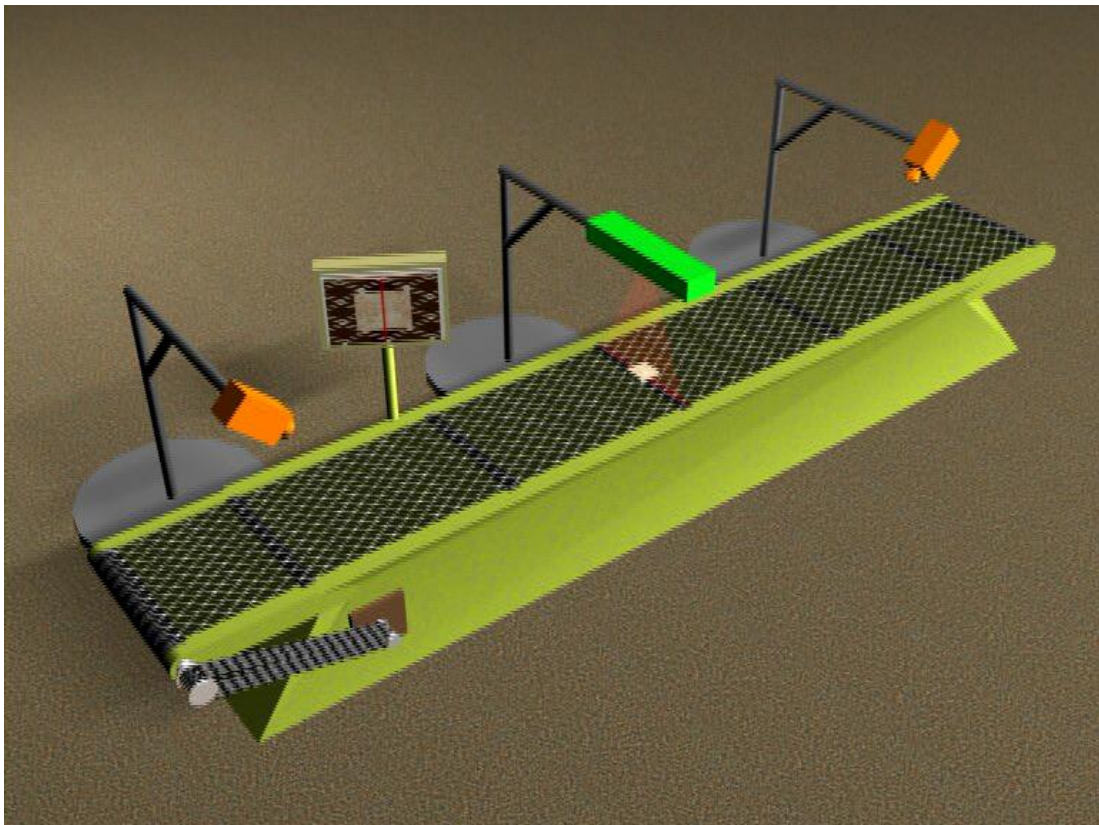


Figure 4.11 Illustration of the 3D image acquisition system (bright green object is laser source, orange objects are cameras).

Different models are designed and realized to create the desired imaging system. The first version of the imaging system is built using Symbol (Motorola[®]) LS2208 (reading distance of 40 cm, 650 nm Laser Diode Light Source and Read Speed: 100 scans / second) barcode reader (laser source), Fujifilm[®] FinePix S5600 (5.22 Mp

resolution, maximum resolution is 2592x1944, minimum resolution is 640x480, sensor type Super CCD IV HR) digital camera and Lego[®] Brainstorm kit (that is used for conveying system) (Figure 4.12). There are some drawbacks for this system. The laser illumination is not constant since the barcode reader's laser is switching to stand-by-state in 1 minute after it has been activated. In addition, one camera is insufficient for the 3D imaging process.



Figure 4.12 Laser based 3D imaging system V.1.

In the second design for a 3D imaging system, a conveyer belt, which is controlled by a step motor, is assembled (Figure 4.13). The size of it is 50 cm long, 30 cm wide. Two webcams (IC-467PLUS (1280 x 960 image processor (1.3 MP), 640 x 480 image sensor (300k) and the Video Power software, 2816 x 2112 (6 MP) resolution photo capture, the CMOS sensor), manufactured by Inca[™], are used. The main drawbacks of this imaging system are that webcam's resolution is low; also, webcams are placed away from the aggregate that is to be scanned. In addition, weight of conveyor belt system is 13.5 kg, so, it cannot be moved easily.



Figure 4.13 Laser based 3D imaging system V.2.

In this work, third and final version of the conveyor belt for imaging system is constructed. It is 25x30 cm in dimension (width, length), and driven by a step motor (Figure 4.14). A laser source that is C13635-2-3(5) type (manufactured by Huanic Corporation) is used. It has 650 nm wavelength, red line module and with a line thickness ≤ 1.5 mm that is made thin to 0.3 mm using 5 degree hypermetropic glass. Two cameras (Logitech[®] Quickcam Pro 9000 which has 2-mega pixel resolution, Carl-Zeiss[®] optics and up to 30 frames per second video capturing property) are attached to two opposite sides of the conveyor belt. Each of them has 45° ($\pm 45^\circ$) viewing angle according to laser source. Laser source is placed 15 cm above the conveyor belt. Webcam and laser source holders are designed to be adjustable. This provides an advantage for positioning related equipment. Aggregates are moved on conveyor belt by a step motor. Step motor has specific run (100 ms because of laser line thickness) and hold on durations (2 sec because of stabilization time of conveyor belt). During the stopping period, line of laser source falls onto aggregate particle and at the same time two webcams capture images from both sides. In this way, two different images (one for each camera) are acquired for a single laser scan line.



Figure 4.14 Laser based 3D imaging system V.3.

4.3.3.2 Calibration

Different objects (triangular prism, cube, and rectangular prism), which are cut from wood and painted with black color, are used for calibration of imaging system. Triangular prism is equilateral, the base length is 2 cm and height from base is 1 cm. Each edge of the cube has length of 1 cm. Rectangular prism's dimensions are 3 cm x 1 cm x 1 cm. Calibration objects and their reconstructed 3D upper side surfaces are shown in Figure 4.15.

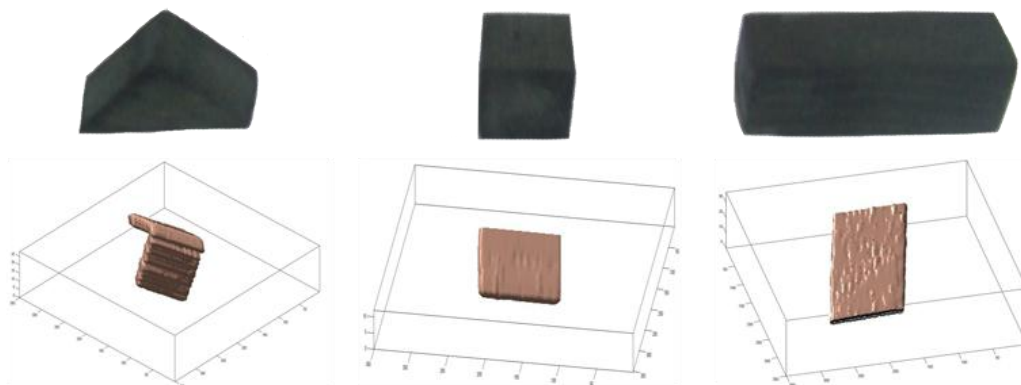


Figure 4.15 Calibration objects and their reconstructed 3D upper side surfaces.

There are 2.54 centimeters per inch and DPI is the resolution in dots per inch, so the formula is rather simple:

$$\text{Centimeters} = \frac{\text{pixels} * 2.54}{\text{DPI}} \quad (4.1)$$

As shown in Table 4.5, L, S and I values are calculated by Equation 4.1 (DPI = 96). There is a difference between real dimensions and measured dimensions. This difference spans between -0.03 cm and +0.1 cm. On the edges, scattered laser light affected the measurement in a negative way. As a result, dimensions showed the given error values.

Table 4.5 L, S and I values of calibration materials.

Prism Type	L (cm)	S (cm)	I (cm)
Cubic	1.10	1.10	0.97
Triangular	1.98	1.01	0.97
Rectangular	3.10	1.10	1.10

4.3.3.3 Image Preprocessing

Preprocessing is accomplished on image slices using Image Processing Toolbox of Matlab[®] software. First, the captured image (resolution of 960x720 pixels) is cropped to specific coordinate values for segmentation. After that, image is converted to gray scale and then thresholded to obtain a binary image. Noise artifacts are removed by eliminating areas having less than 50 pixels for a correct labeling. Example output of the preprocessing is given in Figure 4.16. Image slices give values of distance information on X-Y-Z coordinate plane. Thus, this work is independent from rotation, scale, translation. Rotation of an aggregate does not have any affect as long as the scanned side of the sample remains same. Keeping the distance between camera and aggregate in certain limits, resolution and image quality will be enough for scale invariance. Effect of lateral position change is zero if aggregate stays in the scanning area. Translation on the longitudinal direction has also no effect since this movement is mandatory for 3D scanning process and conveyor belt provides this.

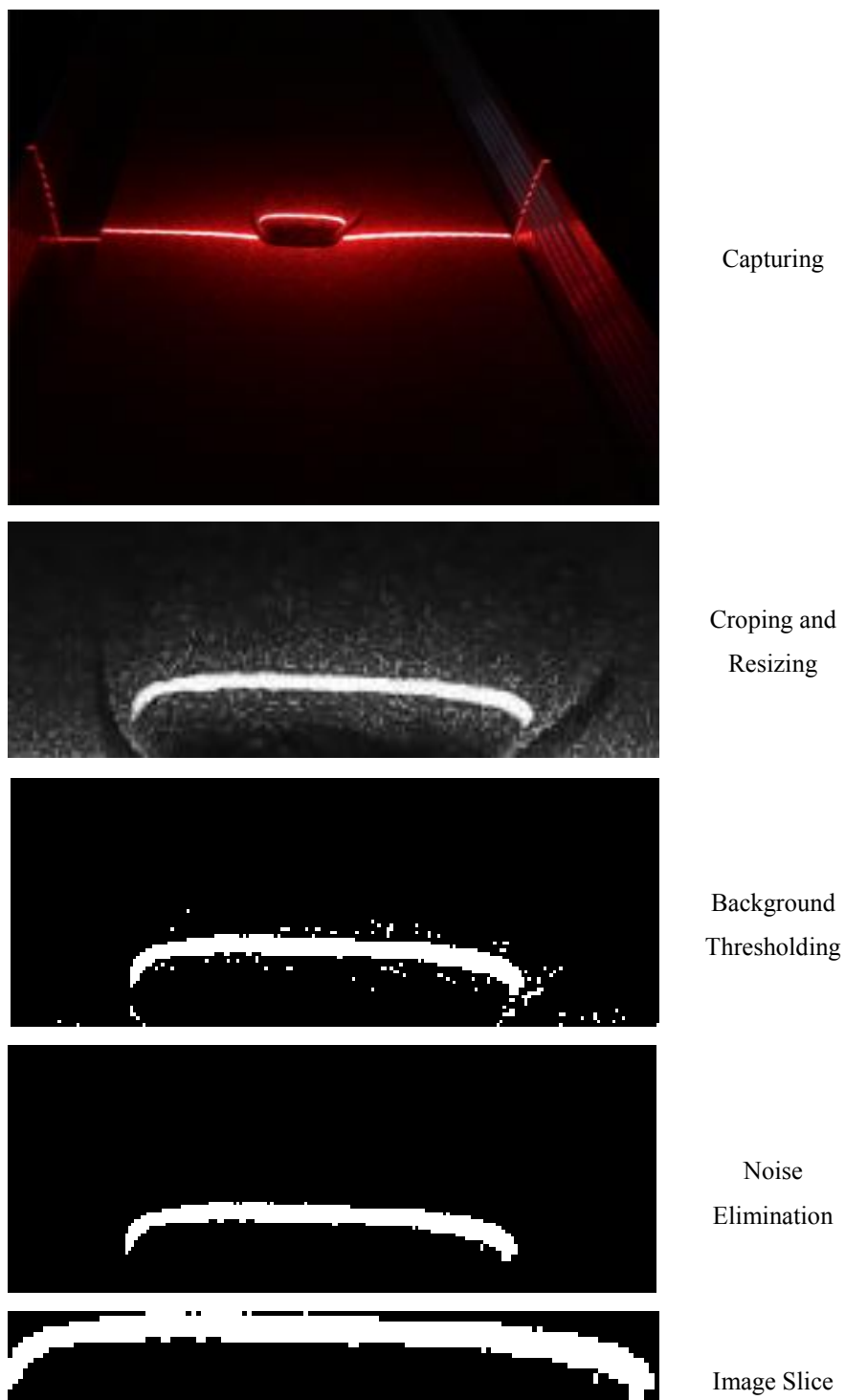


Figure 4.16 Image preprocessing steps.

After preprocessing, image slices are merged to form the upper part 3D image of the sample aggregate (Figure 4.17). The center line is determined by subtracting the

image slices taken from the both angles with two cameras. For this operation, images acquired by the left-camera are rotated 180° with respect to vertical axis (since left-camera looks to the aggregate from the opposite direction), and they are subtracted from the right-camera images. As shown in Figure 4.18, if the number of pixels in the difference image is less than 1% of the total number of pixels of that image slice, second part of aggregate is created using the images of the second camera. This procedure is very important to calculate the real size of the each aggregate sample.

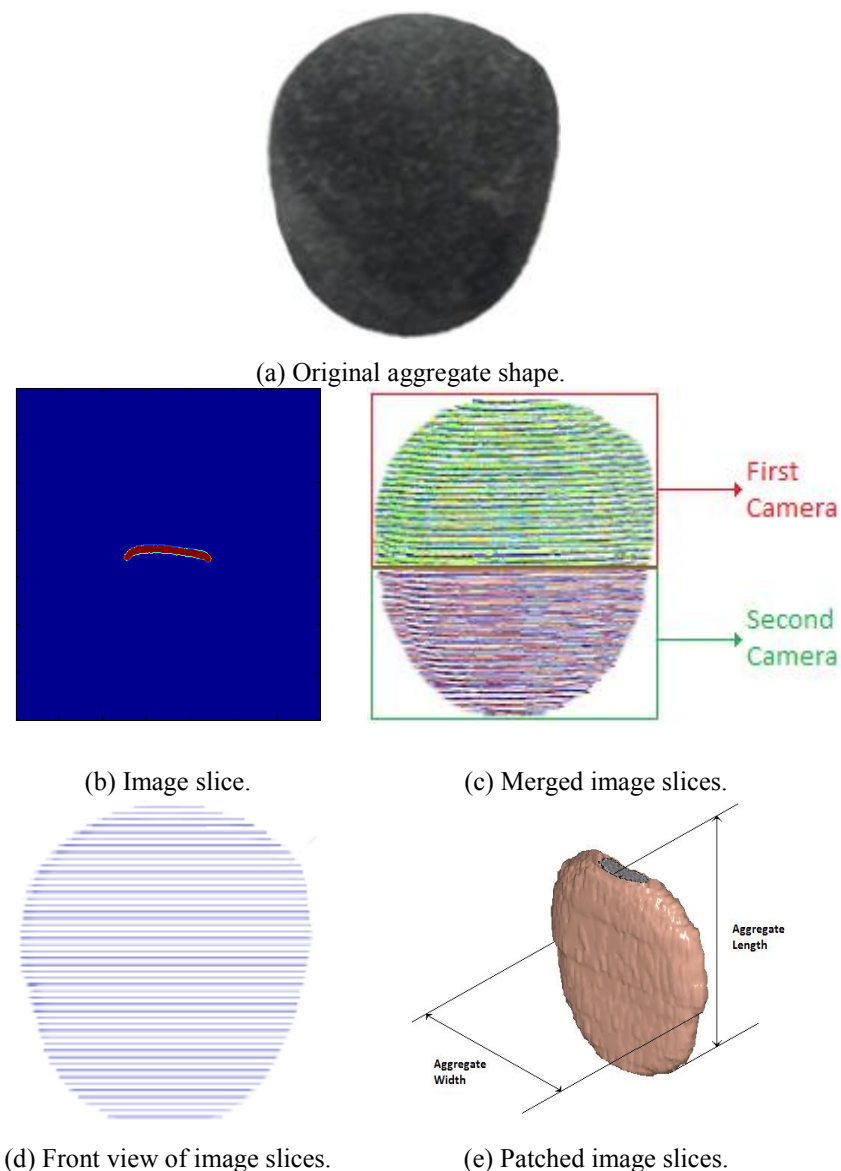


Figure 4.17 Merging slice images of an aggregate and patching the surface as 3D image.

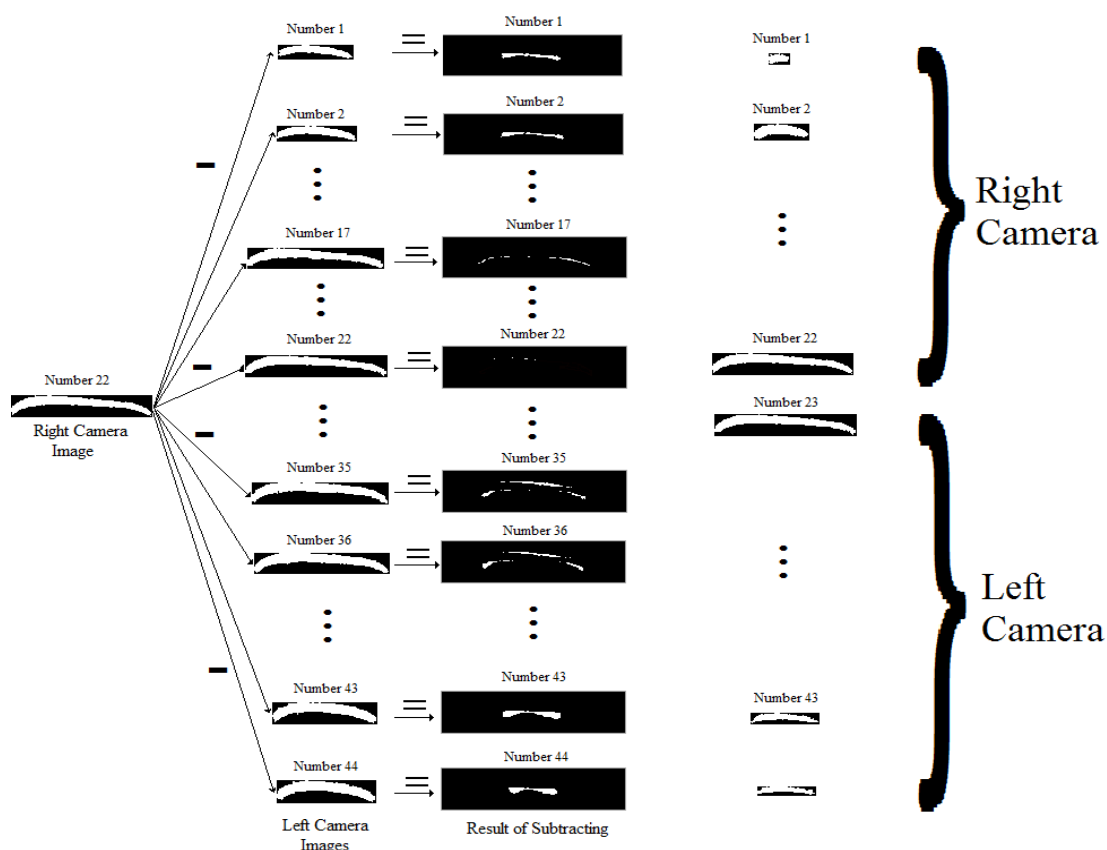


Figure 4.18 Finding center line from image slice.

4.3.3.4 Feature Extraction

Shape properties are important for characterization of aggregates. Shape indexes for aggregates are mainly shape factor, sphericity, flatness, and elongation that are calculated by Equations 1.1-1.4. Three-dimensional information (Long [L], Intermediate [I], and Short [S]) are needed for aggregate characterization. Although these properties are not easily measured by mechanical or manual test methods, in this study 3D information is calculated easily in a short time. Some features are calculated as variations of L, S and I measurements. The software is written in C# for in this work and used to distinguish principal dimensions of the aggregate. It also calculates shape factor, sphericity, flatness, and elongation values.

As shown in Figure 1.2, the L, S and I values are calculated to test our 3D image analysis system. Aggregates are not completely seen because of the limited viewing

angle of the cameras. Therefore, real size of aggregates cannot be calculated correctly when single camera captures images. The results of left, right camera and combination of them are calculated one by one as shown in Table 4.6. Two images (acquired by left and right cameras) of a scan line provide more information than an image of a single camera which yields a measurement with higher accuracy.

Laser line on left and right side edges of some aggregates cannot be correctly viewed by both of the cameras resulting incorrect L measurements. Laser line scattering and occlusion (of laser line by a raised part of the aggregate) can also affect the measurement accuracy.

Table 4.6 Aggregate measurement results (cm).

No	Class	3D Measurement (Two Cameras)			3D Measurement (Left Camera)			3D Measurement (Right Camera)		
		L	S	I	L	S	I	L	S	I
1	Elongate	2.8	0.9	1.7	2.8	0.9	1.8	2.8	0.9	1.8
2	Elongate	1.7	0.9	0.9	1.7	0.9	1.0	1.6	0.9	0.9
3	Elongate	1.8	0.8	0.9	1.8	0.8	0.9	1.8	0.7	0.9
4	Elongate	2.1	0.6	1.1	2.1	0.6	1.2	2.0	0.6	1.2
5	Elongate	2.9	0.8	1.8	2.9	0.8	1.8	2.8	0.7	1.7
6	Elongate	3.7	1.1	1.5	3.7	1.1	1.5	3.8	1.1	1.4
7	Flat	2.7	0.9	2.2	2.7	0.9	2.1	2.8	0.9	2.2
8	Flat	2.3	0.9	2.3	2.2	0.8	2.2	2.3	0.9	2.3
9	Flat	2.3	0.5	1.8	2.2	0.5	1.8	2.3	0.5	1.8
10	Flat	1.6	0.7	2.1	1.5	0.7	1.9	1.6	0.6	2.1
11	Flat	2.0	0.6	1.7	1.8	0.6	1.6	2.0	0.6	1.7
12	Flat	1.3	0.6	1.2	1.3	0.5	1.2	1.3	0.6	1.1
13	Angular	2.0	1.9	2.0	2.0	1.9	2.0	2.0	1.9	1.8
14	Angular	3.8	2.1	1.8	3.7	2.1	1.8	3.8	2.1	1.7
15	Angular	2.6	1.8	1.8	2.5	1.8	1.7	2.6	1.8	1.8
16	Angular	1.9	1.2	1.7	1.9	1.1	1.6	1.8	1.1	1.7
17	Angular	3.1	1.7	1.4	2.8	1.5	1.4	3.1	1.7	1.4
18	Angular	2.3	1.3	1.5	2.1	1.1	1.5	2.3	1.3	1.5
19	Sphere	2.3	2.3	2.3	2.3	2.0	2.2	2.4	2.3	2.3

No	Class	3D Measurement (Two Cameras)			3D Measurement (Left Camera)			3D Measurement (Right Camera)		
		L	S	I	L	S	I	L	S	I
20	Sphere	1.8	2.0	2.5	1.8	1.9	2.4	2.2	2.0	2.5
21	Sphere	1.6	1.4	1.6	1.6	1.4	1.6	1.5	1.4	1.6
22	Sphere	1.8	1.4	1.9	1.8	1.4	1.9	1.8	1.3	1.8
23	Sphere	1.9	2.0	2.0	1.9	1.9	2.0	1.9	2.0	2.0
24	Sphere	1.3	1.0	1.3	1.1	1.0	1.3	1.3	1.0	1.3
25	Round	1.6	1.1	1.4	1.6	1.0	1.4	1.6	1.1	1.6
26	Round	1.7	0.6	1.4	1.7	0.6	1.4	1.7	0.6	1.3
27	Round	1.2	0.5	1.2	1.2	0.5	1.2	1.2	0.5	1.2
28	Round	1.5	0.9	1.2	1.4	0.9	1.2	1.5	0.9	1.2
29	Round	1.3	0.8	1.1	1.3	0.8	1.1	1.3	0.7	1.1
30	Round	1.2	1.0	1.0	0.9	1.0	1.0	1.2	1.0	1.0
31	Formless	1.9	1.2	1.3	1.9	1.2	1.3	1.7	1.2	1.3
32	Formless	1.4	0.9	1.0	1.4	0.9	1.0	1.3	0.9	1.0
33	Formless	1.2	1.8	1.5	1.2	1.8	1.4	1.2	1.8	1.5
34	Formless	2.4	1.8	2.1	2.3	1.5	2.1	2.4	1.8	2.1
35	Formless	1.8	1.4	1.4	1.8	1.4	1.4	1.7	1.4	1.4
36	Formless	2.4	1.9	1.4	2.3	1.9	1.3	2.4	1.9	1.3

In this section, shape features are described and their equations are given (Equation 4.2 – 4.16). Average of sphericity, shape factor, elongation and flatness vectors of all aggregates (2220 samples) are shown in Table 4.7.

- Sphericity is defined as the ratio of particle with sphere diameter of equivalent volume and smallest sphere diameter that is surrounding of particle.

$$Sphericity = \sqrt[3]{\frac{S * I}{L^2}} \quad (4.2)$$

- Shape factor is a commonly used index but different researchers adopt different definitions for it to describe different aspects of shape.

$$\text{Shape Factor} = \frac{S}{\sqrt{L * I}} \quad (4.3)$$

- The elongation ratio is defined as the length to short ratio.

$$\text{Elongation Ratio} = \frac{L}{S} \quad (4.4)$$

- Flatness ratio is defined as the thickness to short ratio.

$$\text{Flatness Ratio} = \frac{S}{I} \quad (4.5)$$

Table 4.7 Average of feature vector values of all aggregates.

No	Class	Sphericity	Shape Factor	Elongation	Flatness
1	Elongate	0,69470	0,97096	2,11041	1,40182
2	Flat	0,63852	1,54659	3,35289	2,83787
3	Angular	0,79489	1,04596	1,67019	1,35399
4	Sphere	0,85826	0,94190	1,35496	1,07842
5	Round	0,74015	1,12276	2,13063	1,63272
6	Formless	0,78390	1,13132	1,86013	1,54728

- Averaged Minimum Height; mean value of minimum height to base line of the aggregate slice (Figure 4.19),

$$\text{Averaged Min Height} = \frac{1}{n} \sum_{i=1}^n (\text{min_hei})_i \quad (4.6)$$

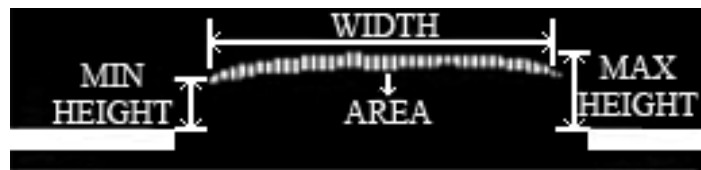


Figure 4.19 Features on the image slice.

- Averaged Maximum Height; mean value of maximum height to base line of the aggregate slices (Figure 4.19),

$$\text{Averaged Max Height} = \frac{1}{n} \sum_{i=1}^n (\max_hei)_i \quad (4.7)$$

- Area; total value of area of the aggregate slices (Figure 4.19),

$$\text{Area} = \sum_{i=1}^n A_i \quad (4.8)$$

- Length; total number of the aggregate slices,

$$\text{Length} = n \quad (4.9)$$

where, n is the total number of the aggregate slices, i is the i^{th} slice, A_i is the area of i^{th} aggregate slice, $(\min_hei)_i$ is the minimum height of i^{th} aggregate slice, $(\max_hei)_i$ is the maximum height of i^{th} aggregate slice.

- Slice Area; area under image slice (Figure 4.20),

$$\text{Slice Area} = \sum_{j=1}^m p_j \quad (4.10)$$

Where p_j is a pixel on an image slice corresponding to the point with minimum height of a laser reflecting surface part. Image slice consists of a set of p_j 's, $\{p_1, p_2, p_3, \dots, p_m\}$, and m is the width of the image slice (in units of pixel).

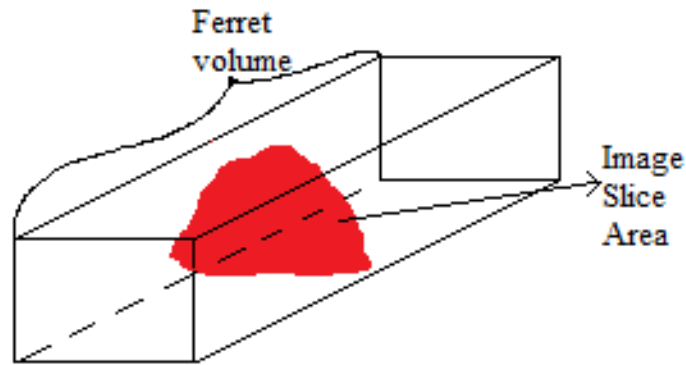


Figure 4.20 Ferret features.

- Image Volume; total area under slice of aggregate (Figure 4.20),

$$\text{Image Volume} = \sum_{i=1}^n (\text{Area Slice})_i \quad (4.11)$$

- Maximum Ferret Area, maximum of bounding box area of aggregate slices (Figure 4.20),

$$\text{Maximum Ferret Area} = \max(\text{rectangle area}_i) \quad (4.12)$$

- Ferret volume, bounding box area of aggregate slice multiplied by total number of aggregate slices (Figure 4.20),

$$\text{Ferret Volume} = n * \text{Maximum Ferret Area} \quad (4.13)$$

- Mean of 3D distance (μ) is the average of the distance between the center of mass and surface pixels of the aggregate,

$$\mu = \frac{1}{k} \sum_{i=1}^k d_i \quad (4.14)$$

Where d_i is Euclidean distance between center of mass and i^{th} surface pixel that is defined by:

$$d_i = \sqrt{(x_c - x_i)^2 + (y_c - y_i)^2 + (z_c - z_i)^2} \quad (4.15)$$

Where x_c, y_c, z_c are center coordinates and x_i, y_i and z_i are coordinates of surface pixels, k is the total pixel number.

- S is the standard deviation of distance between the center of mass and surface pixels of the aggregate (Figure 4.21).

$$S = \sqrt{\frac{1}{k} \sum_{i=1}^k (d_i - \mu)^2} \quad (4.16)$$

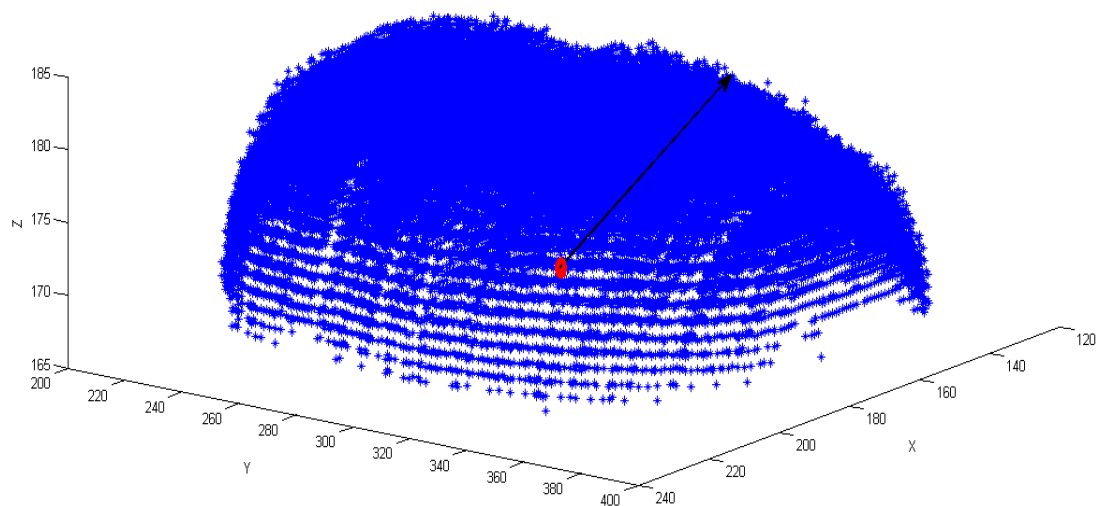


Figure 4.21 3D distance is shown from center point of aggregate to a surface pixel.

4.4 Classification

The aim of classification is to discriminate six different aggregate shape types using aggregate features. Two different artificial neural network models (multilayer perceptron, radial basis function) (Figure 4.22), linear discriminant analysis and k-nearest neighbor methods are used for classification. Each method is described shortly in the following pages. Detailed explanations can be found in the given references.

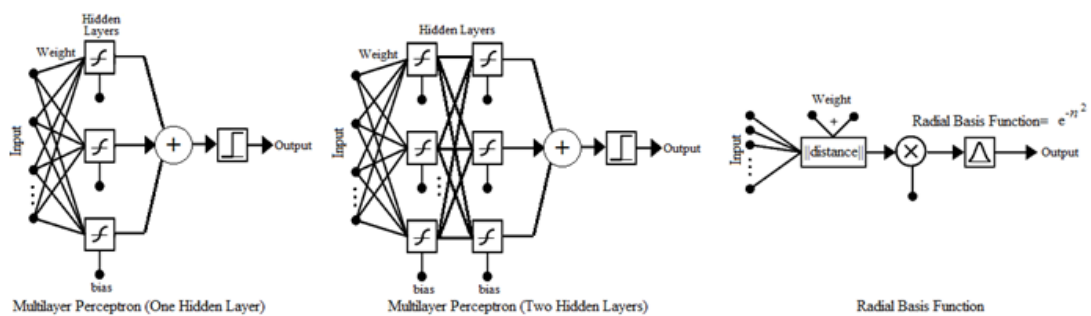


Figure 4.22 Artificial neural network models.

4.4.1 Multi layer perceptron (MLP)

The MLP is a feedforward network which is able to partition the pattern space using nonlinear boundaries for classification problems (Bishop, 1995), (Jain, M., & Mohiuddin, 1996), (Duda, Hart, & Stork, 2000). In this work, two MLP models are used. In the first model (MLP1) there is only one hidden layer, and in the second (MLP2) there are two hidden layers in the network. For both of these layers, the number of nodes are increased one by one from 3 to 15 to calculate the performance percentages of each topology. The network's hidden nodes have tangent sigmoid activation function. Levenberg-Marquardt backpropagation algorithm (Jain, M., & Mohiuddin, 1996) is chosen for training. Gradient descent with momentum weight/bias value is 0.95 for learning function. Mean squared error with regularization value is 0.01 for performance function. The outputs have linear activation functions.

As shown in Figure 4.23, training of MLP1 is stopped when there is 5 validation failures. Maximum training performance (0.015551) is achieved at epoch 142. Training of MLP2 is stopped by the maximum validation failures which is predetermined as 5. Performance reaches to its best value (0.0052132) at epoch 284, as shown in Figure 4.24.

4.4.2 Radial Basis Function (RBF) network

The RBF is special kind of feedforward network which has a high dimensional hidden layer with Gaussian basis (kernels) (Haykin, 1994), (Bishop, 1995), (Jain, M., & Mohiuddin, 1996), (Öztemel, 2003). Output nodes form a linear combination of the basis functions computed by the hidden layer nodes. The basis functions are formed (learned) from the training samples. These basis functions produce a localized response to input stimulus. In this work, spread of RBF is selected as 10 and tolerance for the mean squared error goal value is 1.10^{-9} .

As shown in Figure 4.25, the result of RBF neural network performance is 0.005858 and it is achieved at epoch 550.

4.4.3 Fisher Linear Discriminant Analysis

Fisher linear discriminant analysis (FLDA) finds a linear projection that provides more accurate discrimination between classes. Projections can reduce dimension of the feature vector (Welling, 2006).

4.4.4 K-Nearest Neighbor

K-NN classifies an unlabeled vector through the training examples, each with a class label. Euclidean distance is generally used for calculating nearest k number of training samples to each test sample. The number of neighbors should not exceed the

number of samples (Peterson, 2009), (Değerli, 2011). In this work, k number is selected as 3.

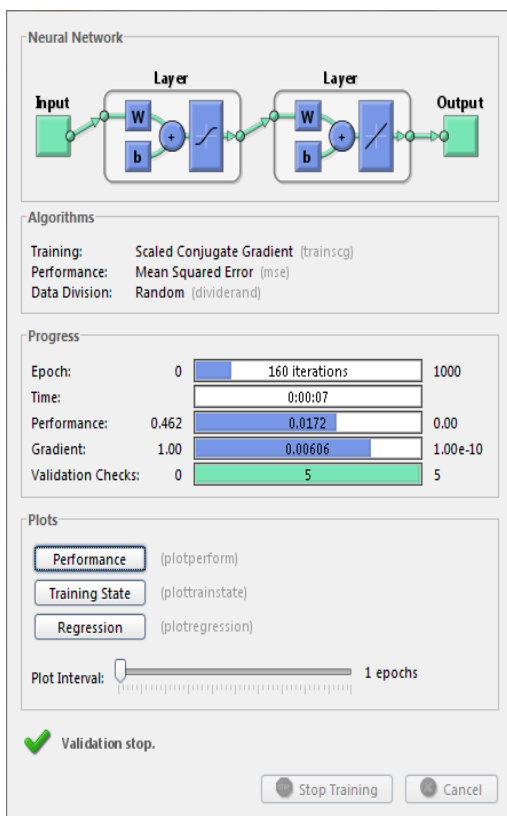
In this work, the inputs (features which are defined in Equation 4.2-4.16) used for training, testing and validation are shown in Table 4.8. Classifier outputs (i.e. aggregate class labels) are given in Table 4.9 as numeric values.

Table 4.8 Input features and mathematical definitions.

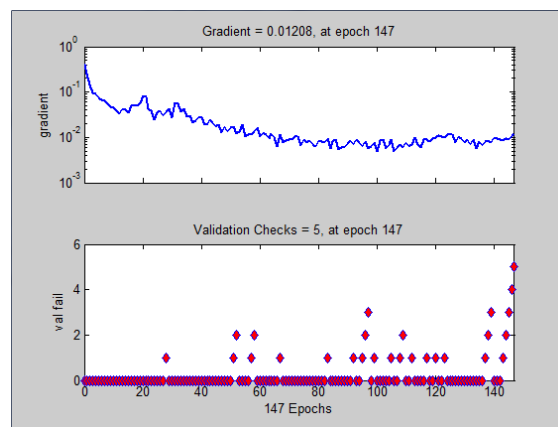
Inputs	Mathematical Definition
Sphericity	$Sphericity = \sqrt[3]{\frac{S * I}{L^2}}$
Shape factor	$Shape\ Factor = \frac{S}{\sqrt{L * I}}$
The elongation ratio	$Elongation\ Ratio = \frac{L}{S}$
Flatness ratio	$Flatness\ Ratio = \frac{S}{I}$
Averaged Minimum Height	$Averaged\ Min\ Height = \frac{1}{n} \sum_{i=1}^n (\min_hei)_i$
Averaged Maximum Height	$Averaged\ Max\ Height = \frac{1}{n} \sum_{i=1}^n (\max_hei)_i$
Area	$Area = \sum_{i=1}^n A_i$
Length	$Length = \sum_{i=1}^n i$
Slice Area	$Slice\ Area = \sum_{j=1}^m p_j$
Image Volume	$Image\ Volume = \sum_{i=1}^n (Slice\ Area)_i$
Maximum Ferret Area	$Maximum\ Ferret\ Area = \max(\text{rectangle area}_i)$
Ferret Volume	$Ferret\ Volume = n * Maximum\ Ferret\ Area$
Mean of 3D distance	$\mu = \frac{1}{k} \sum_{i=1}^k d_i$
Standard deviation of distance	$S = \sqrt{\frac{1}{k} \sum_{i=1}^k (d_i - \mu)^2}$

Table 4.9 Aggregate class labels.

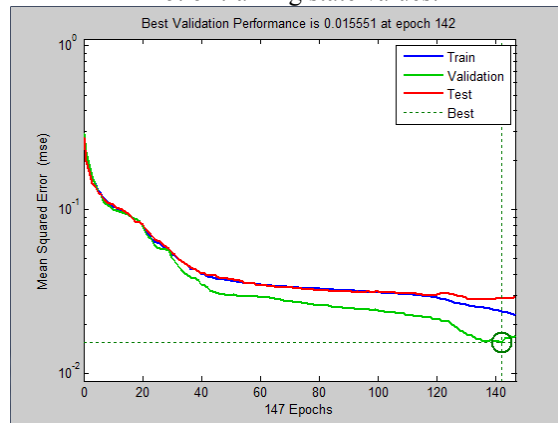
Class Label	Aggregate Definition
1	Elongate
2	Flat
3	Angular
4	Sphere
5	Round
6	Formless



Neural network training.

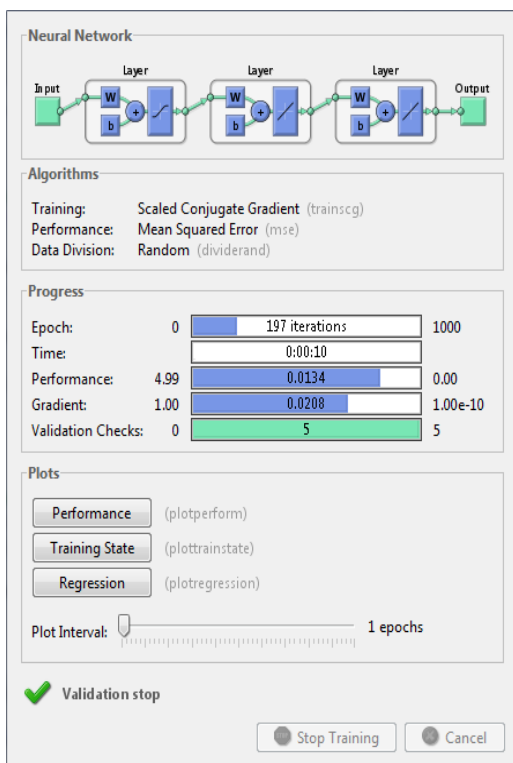


Plot of training state values.

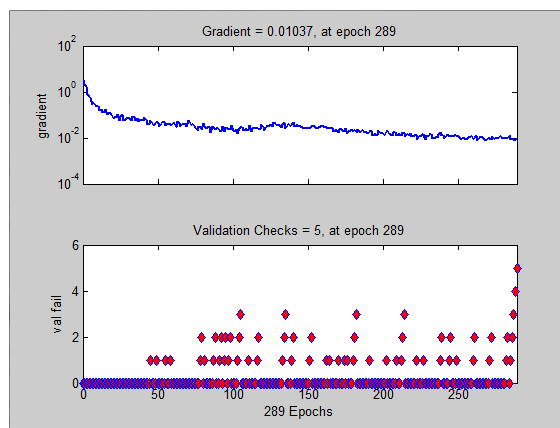


Plot of network performance.

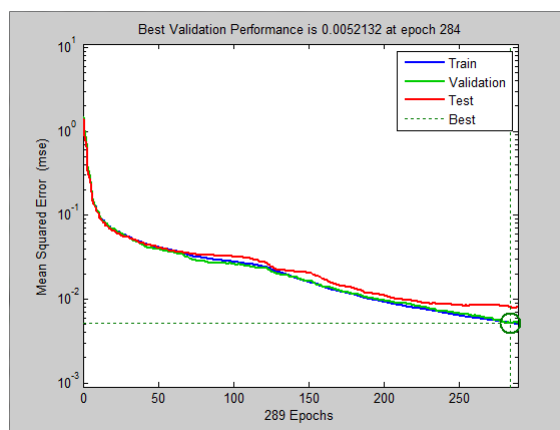
Figure 4.23 Feed forward neural network outputs (one hidden layer).



Neural network training.



Plot of training state values.



Plot of network performance.

Figure 4.24 Feed forward neural network outputs (two hidden layers).

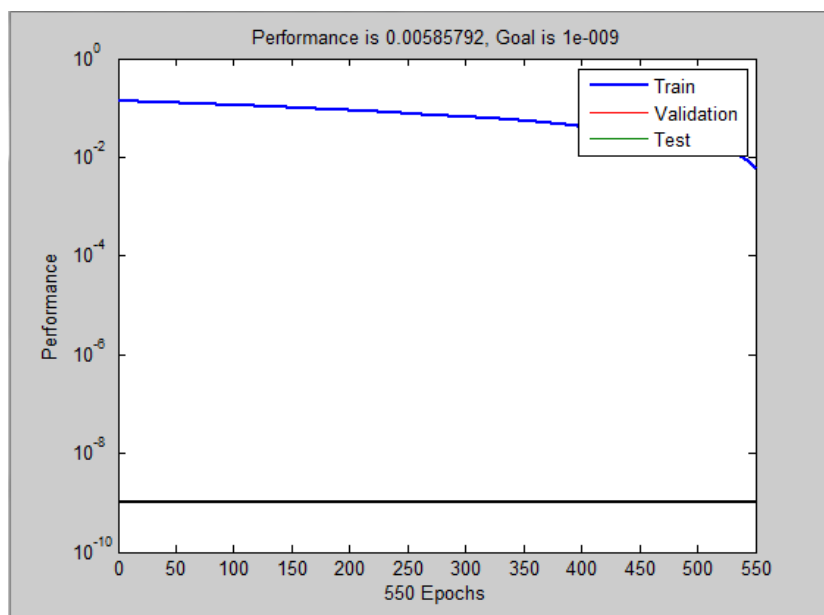


Figure 4.25 Radial basis function neural network performance.

4.5 Results and Discussion

In this study, a new three-dimensional image analysis system that obtains new feature vectors for characterizing six types of different aggregates is developed. The optimal analysis system is created with the experience gathered by using and improving different types of hardware and software components.

The study is evaluated in two stages. In the first step, the developed three-dimensional system is compared both with the manual measurement results and with the two-dimensional image analysis system to identify the advantages of it. Six samples from each of six different aggregate classes are used to compare three methods. Due to the required work for manual measurement is excessive total number of samples is kept small. The L, S and I values of the three methods are shown in Table 4.2, 4.3, 4.6. The disadvantages of manual measurement method are the long measurement times, since every aggregate sample needs to be examined for aggregate projections on graph paper for the top and side views, and requirement for high attention for each aggregate. The disadvantages of the two-dimensional system are manual setup requirement for the acquisition of top and side view aggregate images and environmental conditions (illumination system, camera, shooting range, etc.).

On the other hand, the L, S and I values are directly and easily calculated with merged laser slice images of aggregates by the developed three-dimensional analysis system. In addition, three-dimensional image analysis method simplified the calculation of the volume of aggregate for the scanned (upper) part. Moreover, three-dimensional image analysis system forms the first step for surface texture analysis of the aggregates. This is the most distinctive property of the system.

Second stage of the study is classification work. Six different types of aggregates are classified using the new feature vectors that are obtained through three-dimensional image analysis system. Anova analysis investigates relationships

between feature vectors (McClave, Dietrich II, & Sincich, 1997). Moreover, it analyzes the effects to classes. From these statistical results (Table 4.10) null hypothesis (H_0 : model — which corresponds to extracted 3D feature vector — is useless) is rejected. This means 3D features are suitable for classification. The averaged maximum height, sphericity, long (L) feature vectors have the best discrimination power and they are statistically significant ($p < 0.001$) also as shown in Table 4.11.

Table 4.10 Anova analysis.

Model		Sum of Squares	df	Mean Square	F	Sig.
1	Regression	1355.001	75	90.333	158.344	0.000 ^a
	Residual	401.052	2125	0.570		
	Total	1756.053	2200			

a. Predictors: (constant), sphericity, shape factor, the elongation ratio, flatness ratio, averaged minimum height, averaged maximum height, area, long (L), short (S), intermediate (I), slice area, image volume, maximum ferret area, ferret volume, μ , S

b. Dependent Variable: class

Table 4.11 Statistical analysis results of 3D aggregate features.

Model		Unstandardized Coefficients		Standardized Coefficients	t	Sig.
		B	Std. Error	Beta		
1	(Constant)	-8.007	1.428		-5.609	.000
	Averaged Maximum Height	.083	.003	1.118	25.939	.000
	Averaged Minimum Height	-.035	.007	-.127	-5.196	.000
	Maximum Ferret Area	-1.970E-6	.000	-.130	-1.699	.090
	Area	1.304E-5	.000	.219	4.679	.000
	μ	.031	.018	.183	1.750	.081
	S	-.141	.031	-.356	-4.535	.000
	Long	1.162	.227	.500	5.121	.000
	Short	-1.820	.391	-.573	-4.657	.000
	Intermediate	-.916	.329	-.392	-2.785	.005
	Sphericity	7.725	1.531	.592	5.045	.000
	Shape factor	3.484	1.388	.606	2.510	.012
	Elongation	.328	.297	.188	1.103	.270
	Flatness	-.436	.671	-.206	-.651	.516

a. Dependent Variable: class

Average performance results are given in Table 4.12. The results in confusion matrix (Table 4.13) show that shape parameters of some formless type aggregates are too close to the other aggregate classes. Sphere type aggregates are classified with the best performance (100%) because they naturally have maximum sphericity and their L, S and I values are close the each other.

MLP2 network model has best performance with the accuracy value 99.20%. These results show that it is a positive approach to classify six different types of aggregates using the new feature vector. ROC curves for the neural network

classifiers are given in Figure 4.26. Area under the ROC curve is an important criterion about classifier performance (Table 4.14).

Table 4.12 Classification results (a. Multilayer perceptron with one hidden layer, b. Multilayer perceptron with two hidden layers, c. Radial Basis Function, d. Fisher Linear Discriminant Analysis, e. K-Nearest Neighbor)

<u>Network Type</u>	<u>Node Number (First Hidden Layer)</u>	<u>Node Number (Second Hidden Layer)</u>	<u>(%) Average Performance</u>
MLP1 ^a	8	-	90.40
MLP2 ^b	15	15	99.20
RBF ^c	-	-	93.79
FLD ^d	-	-	96.20
KNN ^e	-	-	91.39

Table 4.13 Confusion matrix of neural network having best performance (1.Elongate, 2.Flat, 3.Angular, 4.Sphere, 5.Round, 6.Formless).

		Target Class						
		1	2	3	4	5	6	
Output Class	1	228	0	0	0	0	3	98.7 %
		10.3 %	0.0 %	0.0 %	0.0 %	0.0 %	0.1 %	1.3 %
	2	3	447	0	0	0	0	99.3 %
		0.1 %	20.2 %	0.0 %	0.0 %	0.0 %	0.0 %	0.7 %
	3	0	0	297	0	0	0	100 %
		0.0 %	0.0 %	13.4 %	0.0 %	0.0 %	0.0 %	0.0 %
	4	0	0	0	435	0	0	100 %
0.0 %		0.0 %	0.0 %	19.7 %	0.0 %	0.0 %	0.0 %	
5	0	0	0	0	519	6	98.9 %	
	0.0 %	0.0 %	0.0 %	0.0 %	23.4 %	0.3 %	1.1 %	
6	0	0	6	0	0	267	97.8 %	
	0.0 %	0.0 %	0.3 %	0.0 %	0.0 %	12.1 %	2.2 %	
		98.7 %	100 %	98.0 %	100 %	100 %	96.7 %	99.2 %
		1.3 %	0.0 %	2.0 %	0.0 %	0.0 %	3.3 %	0.8 %

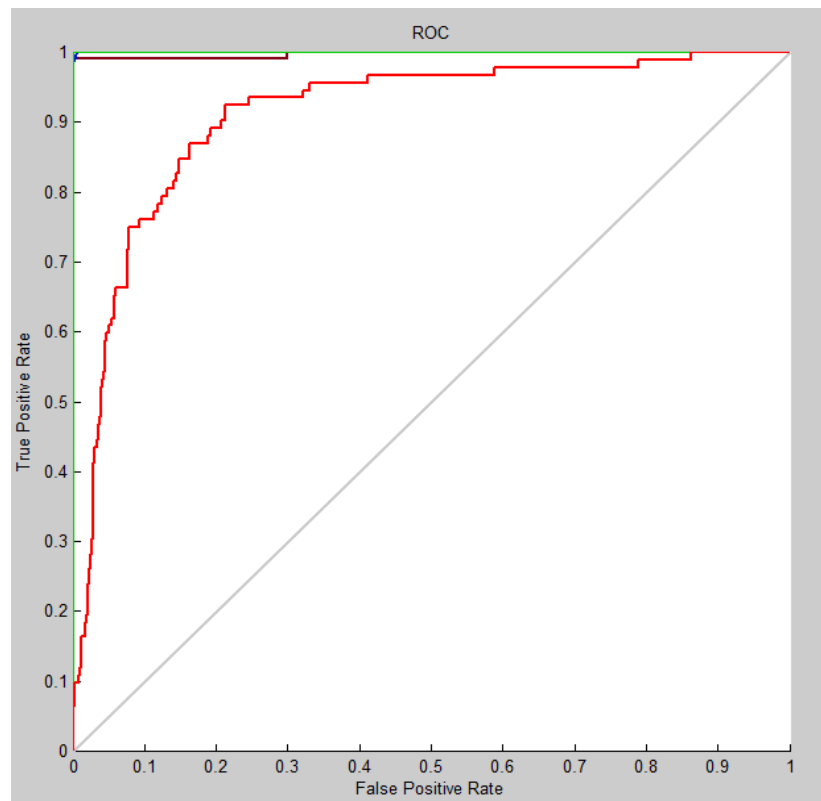


Figure 4.26 ROC curve.

Table 4.14 Area under the ROC curve.

Class	Area Under the Curve
Elongate	0.9998
Flat	1.0000
Angular	0.9970
Sphere	1.0000
Round	1.0000
Formless	0.9094

In Table 4.15, the aggregates are classified into two groups as well-shaped and poor-shaped (Joret, Isa, Ali, Zamli, Azizli, & Batah, 2005). The aggregates are defined poor-shaped, if L/S ratio is more than 3 (Ünal, 2011). These type of aggregates are generally flat and elongate. Other type of aggregates are defined well-shaped. The confusion matrix shows that MLP2 classify with the rate of 99.90%. Area under the ROC curve is calculated as 0.9922 (Figure 4.27).

Table 4.15 Confusion matrix of well-shaped and poor-shaped aggregates (1. Poor-shaped (elongate and flat), 2. Well-shaped (angular, sphere, round, formless)).

		Target Class		
		1	2	
Output Class	1	678 30.6	3 0.1%	99.6% 0.4%
	2	0 0.0 %	1539 69.3%	100 % 0.0 %
		100 % 0.0 %	99.8% 0.2%	99.9% 0.1%

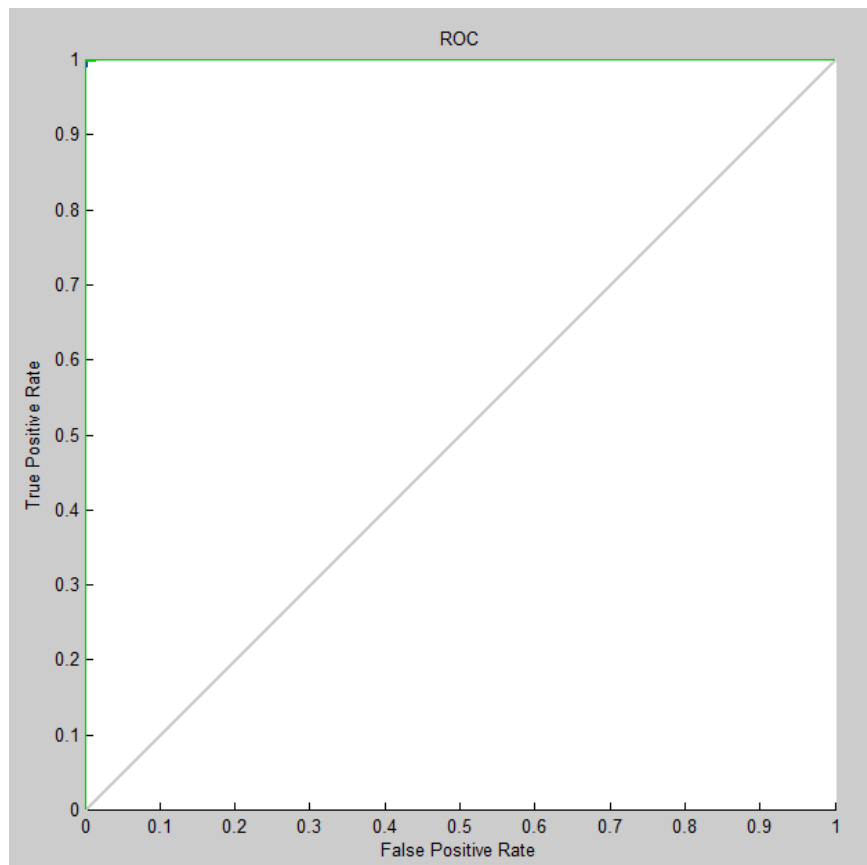


Figure 4.27 ROC curve of well-shaped and poor-shaped aggregate classifier.

In this chapter, material and methods are investigated. Developed 3D imaging system is explained and compared. The new features are formularized and statistically analyzed. Then they are used for classification. Classification performance is measured. Results are discussed. In following chapter, this work is concluded.

CHAPTER FIVE

CONCLUSIONS AND SUGGESTIONS FOR FUTURE WORK

5.1 Conclusions

In this thesis work, 3D imaging system has been designed for the characterization and classification of aggregates that are grouped under six basic categories. 3D feature vectors are extracted in this process. Analysis of these features revealed that they have high discrimination power, which yielded successful classification results.

The quality of aggregate directly affects the fresh concrete and its workability. Cement and water requirements and strength and durability of hardened concrete are also affected. Because of this reasons, determination of defective aggregate types (flat and elongate) is very important. Our system performed quite successful in this classification process with 99.90%. In addition, our system classified six type aggregates as the elongate, flat, angular, sphere, round and formless with 99.20%.

We extracted the new feature vectors for shape characterization and classification of aggregate by efficiently utilizing the developed 3D imaging system. The averaged maximum height, sphericity, long feature vectors have the best discrimination power and statistically significant ($p < 0.001$). The averaged minimum height, short and 3D distance standard deviation feature vectors have the minimum discrimination power, though they are statistically significant.

Averaged maximum height value of flat aggregate is generally similar since flat surface is only distorted at the edges which has a minimum effect on the feature. On the other hand, sphere aggregate has maximum value for this feature because of its surface geometry shows only change in a circular area. Formless aggregates, which are irregular, have different values of this feature. In generally this feature has the best discrimination power (statistically significant ($p < 0.001$)).

In this work, we used different classifier models (artificial neural network, fisher linear discriminant and k-nearest neighbor). Multi-layer perceptron neural network model, which has two hidden layers, provides the best discrimination. This shows that mathematical model (extracted 3D features) of aggregates fits to the model of the nonlinear classifier. In other words, feature space (with sixteen dimensions) is nonlinearly partitioned by the selected multi-layer perceptron neural network giving high classification performance.

We designed different 3D laser based imaging systems to minimize error during capturing images of aggregates. The first two designs had different problems as mentioned previously. We improved designs to realize the optimal 3D laser imaging system. This process was continued about 1.5 years.

Software has been developed using C# programming language. Step motor motion control system, imaging system and digital image storage system has been implemented. Required library files are created in Matlab® program and integrated to C# software. This program controls the capturing process. Captured images are processed and 3D shape features are extracted from them in a short time (with a maximum duration 65 seconds). We have written 3725 lines of code that contains capturing, preprocessing, reconstruction, feature extraction and classification processes.

As a result, when compared with the works of others (Garboczi, 2002), (Fernlund, 2005), (Lee, Smith, & Smith, 2007), our system is fast, cheap and easy to use. Novel features of six different types of aggregates provide higher classification results than the performance achieved in work of Al-Batah, et al. (2009). Our system can easily measure the shape parameters of the aggregates which makes it highly preferable to traditional methods (Anonymous, UTEST Material Testing Equipment, 2011), (Anonymous, ASTM International Standards Worldwide - Home, 2011).

5.2 Suggestions for Future Work

Presented work is a step towards an advanced automation system for classification of the aggregates based on 3D shape parameters. Further studies are going to be related with the system performance enhancement, including new 3D shape parameters of aggregates. Quality control in building construction area can be done using this system. Thus, quantitative quality measurement of aggregate can be accomplished during concrete production. The aim of the next phase of this work is to enhance the classification system by including new aggregate samples. Moreover, the future works may include the surface roughness parameters of aggregate to improve the main idea of this thesis.

REFERENCES

- Al-Awadhi, F., Hurn, M., & Jennison, C. (2011). Three dimensional statistical image analysis and confocal microscopy. *Journal of Applied Statistics*, 29-46.
- Al-Batah, M. S., Isa, N. A., Zamli, K. Z., Sani, Z. M., & Azizli, K. A. (2009). A novel aggregate classification technique using moment invariants and cascaded multilayered perceptron network. *International Journal of Mineral Processing* (92), pp. 92-102.
- Al-Rousan, T. (2004). Ph.D. Disertation. *Characterization of aggregate shape properties using a computer automated system*. Texas: A&M University, College Station, TX.
- Al-Rousan, T., Masad, E., Tutumluer, E., & Tongyan, P. (2007). Evaluation of image analysis techniques for quantifying aggregate shape characteristics. *Construction and Building Materials* (21), pp. 978–990.
- Anonymous. (2002). *Renishaw Inc*. Retrieved 2011, from Heterodyne and Homodyne Interferometry: [http://resources.renishaw.com/en/Homodyne+and+heterodyne+interferometry\(5653\)](http://resources.renishaw.com/en/Homodyne+and+heterodyne+interferometry(5653))
- Anonymous. (2006, September 15). *Confocal laser scanning microscopy*. Retrieved May 12, 2011, from Wikipedia: http://en.wikipedia.org/wiki/Confocal_laser_scanning_microscopy
- Anonymous. (2009, October 8). *3D Forums*. Retrieved April 25, 2011, from Stereoscopic Parallax: <http://www.3d-forums.com/stereoscopic-parallax-t4.html>
- Anonymous. (2010, April 10). *Anaglyph image*. Retrieved April 26, 2011, from Wikipedia: http://en.wikipedia.org/wiki/Anaglyph_image
- Anonymous. (2011). *Interferometry*. Retrieved from Wikipedia: <http://en.wikipedia.org/wiki/Interferometry>

- Anonymous. (2011). *3D Laser Imaging & Profile*. Retrieved 2011, from Invisuale E. Inc.: <http://www.invisuale.com/3d-laser.html>
- Anonymous. (2011). *3D scanner*. Retrieved from Wikipedia: http://en.wikipedia.org/wiki/3D_scanner
- Anonymous. (2011). *Aggregate*. Retrieved from Cement & Concrete Basics: http://www.cement.org/basics/concretebasics_aggregate.asp
- Anonymous. (2011). *ASTM International Standards Worldwide - Home*. Retrieved 2011, from ASTM C1252 - 06: <http://www.astm.org/Standards/C1252.htm>
- Anonymous. (2011). *Computer Vision*. Retrieved from Wikipedia: http://en.wikipedia.org/wiki/Computer_vision
- Anonymous. (2011). *Gradation Test*. Retrieved from Pavement Intractive: http://pavementinteractive.org/index.php?title=Gradation_Test
- Anonymous. (2011). *INDOT*. Retrieved from Aggregate Properties: www.in.gov/indot/files/chapter_03.pdf
- Anonymous. (2011). *Integrated Publishing*. Retrieved 2011, from Uncompacted voids in aggregates (ASTM C 1252): http://www.tpub.com/content/ArmyCRREL/SR99_20/SR99_200013.htm
- Anonymous. (2011, April 5). *Interferometry*. Retrieved April 23, 2011, from Wikipedia: <http://en.wikipedia.org/wiki/Interferometry>
- Anonymous. (2011). *Sieve Analysis*. Retrieved from Civil Engineering Portal: <http://www.engineeringcivil.com/sieve-analysis.html>
- Anonymous. (2011). *Sieve Analysis*. Retrieved from Wikipedia: http://en.wikipedia.org/wiki/Sieve_analysis
- Anonymous. (2011, April 30). *Stereoscopy*. Retrieved May 25, 2011, from Wikipedia: <http://en.wikipedia.org/wiki/Stereoscopy>

- Anonymous. (2011). *Structured-light 3D scanner*. Retrieved from Wikipedia: http://en.wikipedia.org/wiki/Structured-light_3D_scanner
- Anonymous. (2011). *Surface Roughness Review*. Retrieved from Engineers Edge: http://www.engineersedge.com/surface_finish.htm
- Anonymous. (2011). *UTEST Material Testing Equipment*. Retrieved 2011, from Aggregate General and Geometric Properties: <http://www.utest.com.tr/en/>
- Aschenbrenner, B. (1956). A new method of expressing particle sphericity. *Journal of Sedimentary Petrology*, pp. 15-31.
- Barksdale, R. (1991). Measurement of Aggregate Shape, Surface Area, and Roughness. *Transportation Research Record*, pp. 107-116.
- Barksdale, R. D., & Itani, S. Y. (1994). Influence of aggregate shape on base behavior. *Transportation Research Record (1227)*, pp. 171-182.
- Beato, A. (2011, January 13). *Stereo 3D Fundamentals*. Retrieved April 14, 2011, from Affonso Beato Personel Web Page: http://web.me.com/abeato/sd3dcalculator/Stereo_3D_Fundamentals.html
- Benhamou, M., & Clara, F. (1993). Advances in 3D Computer Vision for Neuron Analysis. *Systems, Man and Cybernetics* (pp. pp. 508 – 512). Le Touquet, France: Systems Engineering in the Service of Humans (IEEE).
- Bikerman, J. J. (1964). *Adhesion of asphalt to stone*. USA: MIT Civil Engineering Research Report R64-3.
- Bishop, C. (1995). *Neural Networks for Pattern Recognition*. Great Britain: Oxford University Press.
- Bishop, C. (2006). *Pattern Recognition and Machine Learning*. Singapore: Springer Science.
- Brzezichi, J., & Kasperkiewicz, J. (1999). Automatic image analysis in evaluation of aggregate shape. *Journal of Computing in Civil Engineering (13)*, pp. 123–130.

- Chelliah, V. (1999). EE494/594 Presentation. *Holographic Interferometer*. New York, Buffalo, USA: University at Buffalo.
- Creath, K., & Wyant, J. (2008). Optics 513 Chapter Note. *Moiré and Fringe Projection Techniques*. Arizona, USA: The University of Arizona.
- Çetin, A., & GÜdükbay, U. (2006). 3 Boyutlu Bilgisayar Grafikleri (3D Computer Graphics). In T. Ören, & T. Öney, *Türkiye Bilişim Ansiklopedisi* (pp. 211-220). Ankara: Papatya Yayıncılık.
- Dändliker, R., Salvadé, Y., & Zimmermann, E. (1998). Distance measurement by multiple-wavelength interferometry. *Journal of Optics* (29), pp. 105-115.
- Das, A. (2006). A revisit to aggregate shape parameters. Workshop on Aggregates-flakiness and elongation indices. WSOA.
- Değerli, O. (2011, March 15). *K-Nearest Neighbor Algorithm*. Retrieved 2011, from Onur Değerli Kişisel Sitesi: <http://www.onurdegerli.com.tr/2011/03/15/en-yakin-k-komsu-algoritmasi-k-nearest-neighbor-algorithm/>
- Devarakota, P., Mirbach, B., Castillo-Franco, M., & Ottersten, B. (2005). 3-D Vision Technology for Occupant Detection and Classification. *DIM '05 Proceedings of the Fifth International Conference on 3-D Digital Imaging and Modeling* (pp. pp. 72 – 79). Washington DC: IEEE Computer Society.
- Dilek, U. (2000). Ph.D. Thesis. *Effects of Manufactured Sand Characteristics on Properties Concrete*. North Caroline State University.
- Dipanda, A., Woo, S., Marzani, F., & Bilbault, J. (2003). Shape reconstruction in an active stereo vision system using genetic algorithms. *Kernel and Subspace Methods for Computer Vision* (36) (pp. pp. 2143-2159). Elsevier Science B.V.
- Dipanda, A., Woo, S., Marzani, F., & Bilbault, J. M. (2003). 3-D shape reconstruction in an active stereo vision system using genetic algorithms. *Pattern Recognition*, 2143-2159.

- Dodds, S. (2003). Holographic Interferometry. Physics Department Rice University.
- Dodds, S. (2010). Holographic Interferometry. *Lesson Note of Physics*. Texas, USA: Rice University.
- Dorrington, A. A., Kelly, C. D., McClure, S. H., Payne, A. D., & Cree, M. J. (2009). Advantages of 3D Time-of-Flight Range Imaging Cameras in Machine Vision Applications. *The 16th Electronics New Zealand Conference (ENZCon)*, (pp. 95-99). New Zealand.
- Duda, R., Hart, P., & Stork, D. (2000). *Pattern Recognition (2nd Ed.)*. New York: Wiley-Interscience.
- Erdogan, S., Quiroga, P., Fowler, D., Saleh, H., Livingston, R., Garboczi, E., et al. (2006). Three-dimensional shape analysis of coarse aggregates: New techniques for and preliminary results on several different coarse aggregates and reference rocks. *Cement and Concrete Research (36)*, pp. 1619-1627.
- Erdoğan, T. Y. (2002). *Materials of Construction*. Ankara: Metu Press.
- Erne, O. (2010). *Electronic Speckle Pattern Interferometry: Temporal vs. Spatial Phase-Shifting*. Portland State University.
- Fernlund, J. (2005). 3-D image analysis size and shape method applied to the evaluation of the Los Angeles test. *Engineering Geology (77)*, pp. 57–67.
- Fernlund, J., Zimmerman, R., & Kragic, D. (2007). Influence of volume/mass on grain-size curves and conversion of image-analysis size to sieve size. *Engineering Geology (90)*, pp. 124–137.
- Ferron, A. (2000). Theory and Applications of Digital Image Processing. *Course Note*. Offenburg: University of Applied Sciences.
- Forsyth, D., & Ponce, J. (2002). *Computer Vision: A Modern Approach (1th Ed.)*. USA: Prentice Hall.

- François, A., & Madroni, G. (2001). Interactive 3D Model Extraction from a Single Image. *Elsevier Image and Vision Computing (19)*, pp. 317-328.
- Galloway, J. E. (1994). Grading, Shape and Surface Properties in Significance of Tests and Properties of Concrete and Concrete-Making Materials. *ASTM Special Technical Publication (169)*, pp. 401-410.
- Garboczi, E. (2002). Three-dimensional mathematical analysis of particle shape using X-ray tomography and spherical harmonics: Application to aggregates used in concrete. *Cement and Concrete Research (32)*, pp. 1621–1638.
- Gerhard, H., & Busse, G. (2002). Deformation-Measurement with Speckle-Interferometry by Ultrasound Excitation. *8th ECNDT*. Barcelona: the Spanish Society for NDT.
- Gerhard, H., & Busse, G. (2002). Deformation-Measurement with Speckle-Interferometry by Ultrasound Excitation. *8th ECNDT (8)*. Barcelona: NDT.net.
- GFMesstechnik. (2008). *Structured-light 3D scanner*. Retrieved from Wikipedia: http://en.wikipedia.org/wiki/Structured-light_3D_scanner
- Gokturk, S. B., & Tomasi, C. (2004). 3D head tracking Based on Recognition and Interpolation Using a Time-of-Flight Depth Sensor. *Computer Vision and Pattern Recognition (CVPR'04) (2)* (pp. pp.211-217). Washington: IEEE Computer Society Conference.
- Gokturk, S. B., Yalcin, H., & C., B. (2004). A Time-Of-Flight Depth Sensor – System Description, Issues and Solutions. *Computer Vision and Pattern Recognition Workshop (CVPRW'04) (3)* (pp. pp.211-217). Washington: IEEE Computer Society Conference.
- Gonzalez, R. C., & Woods, R. E. (2002). *Digital Image Processing (2nd Ed.)*. USA: Prentice Hall.
- Gonzalez, R. C., & Woods, R. E. (2005). *Digital Image Processing using Matlab*. USA: Prentice Hall.

- Grossmann, P. (1987). Depth from focus. *Pattern Recognition Letters*, 63-69.
- Haas, C. T., Rauch, A. F., Kim, H., & Browne, C. (2002). *Automation of Aggregate Characterization Using Laser Profiling and Digital Image Analysis*. Washington, D.C.: Aggregates Foundation for Technology, Research, and Education.
- Haykin, S. (1994). *Neural Networks a Comprehensive Foundation*. USA: Macmillan Publishing Company.
- Heijden, F. V., Dain, R. P., Ridder, D. D., & Tax, D. M. (2004). *Classification, parameter estimation and state estimation on engineering approach using Matlab (1th Ed.)*. England: Jhon Wiley&Sons.
- Hudson, B. P. (1995). The Effect of Manufactured Aggregate and Sand Shape on Concrete Production and Placement. *Svedala Barmac New Zealand Limited*, (pp. pp. 1-15).
- Hudson, B. P. (1999). Modification to the fine aggregate angularity test investigation into the way we measure fine aggregate angularity. *Proceedings of the 7th Annual Symposium* (pp. 1-10). Austin: International Center for Aggregate Research (ICAR) Symposium.
- Isa, N. A., Al-Batah, M. S., Zamli, K. Z., Azizli, K. A., Jore, A., & Noor, N. R. (2008). Suitable features selection for the HMLP and MLP Networks to identify the shape of aggregate. *Construction and Building Materials* (22), pp. 402–410.
- Itoh, H., Matsuo, K., Oida, A. N., Miyasaka, J., & Izumi, T. (2008). Aggregate size measurement by machine vision. *Journal of Terramechanics* (45), pp. 137–145.
- Jähne, B. (2002). *Digital Image Processing (5th revised and extended ed.)*. New York: Springer-Verlag Heidelberg.
- Jähne, B., & Haußecker, H. (2000). *Computer Vision and Applications: A Guide for Students and Practitioners (1st ed.)*. USA: Academic Press.

- Jähne, B., Haussecker, H., & Geissler, P. (1999). *Handbook of Computer Vision and Applications*. United States of America: Academic Press.
- Jain, A. K., M., J., & Mohiuddin, K. M. (1996). Artificial Neural Networks: A Tutorial. *IEEE Computer Society* (29), pp. 31-44.
- Jain, R., Kasturi, R., & Schmoh, B. G. (1995). *Machine Vision*. USA: McGraw-Hill.
- Janoo, V. (1998). *Quantification of Shape, Angularity, and Surface Texture of Base Course Materials*. Special Report 98-1.
- Joret, A., Isa, N. A., Ali, A. N., Zamli, K. Z., Azizli, K. A., & Batah, M. S. (2005). Classifying the shape of aggregate using hybrid multilayered perceptron network. *Proceeding ICS'05 Proceedings of the 9th WSEAS International Conference on Systems* (pp. 1-6). USA: The ACM Digital Library.
- Keller, M. (2011). *3D Imaging and Display Techniques*. Retrieved April 26, 2011, from eHow: http://www.ehow.com/list_6662915_3d-imaging-display-techniques.html
- Kim, H., Haas, C. T., & Rauch, A. F. (2002). Image Texture Based Quality Control Of Aggregate Production. *2002 10th Annual Symposium Research Papers* (pp. 1-12). USA: International Center For Aggregates Research (Icar).
- Kim, H., Haas, C. T., & Rauch, A. F. (2003). 3D Image Segmentation of Aggregates From Laser Profiling. *Computer-Aided Civil and Infrastructure Engineering* (18), pp.254-263.
- Kim, H., Haas, C., Rauch, A., & Browne, C. (2002). Dimensional Ratios for Stone Aggregates from 3D Laser Scans. *Journal of Computing in Civil Engineering* (16), pp. 175-183.
- Kim, H., Rauch, A. F., & Haas, C. T. (2002). The Laser-Based Aggregate Scanning System: Current Capabilities and Potential Developments. *International Center for Aggregates Research 10th Annual Symposium: Aggregates - Asphalt*

- Concrete, Portland Cement Concrete, Bases and Fines* (pp. pp. 1-12). Baltimore, Maryland: Transportation Research Board.
- Kim, H., Rauch, A. F., & Haas, C. T. (2002). The Laser-Based Aggregate Scanning System: Current Capabilities And Potential Developments. *International Center for Aggregates Research 10th Annual Symposium: Aggregates - Asphalt Concrete, Portland Cement Concrete, Bases and Fines* (p. 16 p.). Texas: Transportation Research Board.
- Kovács, T. (2004). Creating Morph Targets with an Active. *5th International Symposium of Hungarian Researchers on Computational Intelligence* (pp. 1-10). Budapest: Budapest Tech.
- Krumbein, W. C. (1991). Measurement of geological significance of shape and roundness of sedimentary particles. *Sediment Petrol* (11), pp. 64-72.
- Krumbein, W. C., & Sloss, L. L. (1951). *Stratigraphy and Sedimentation* (2nd Ed.). London: W. H. Freeman and Company.
- Kuo, C. Y., & Freeman, R. B. (2000). Imaging indices for quantification of shape, angularity, and surface texture of fine aggregates. *Journal of the Transportation Research Board*, pp. 57-66.
- Kuo, C. Y., Rollings, R. S., & Lynch, L. N. (1998). Morphological study of coarse aggregates using image analysis. *Journal of Materials in Civil Engineering* (3), pp. 135-142.
- Kwan, A. K., Mora, C. F., & Chan, H. C. (1999). Particle shape analysis of coarse aggregate using digital image processing. *Cement and Concrete Research* (29), pp. 1403–1410.
- Lanaro, F., & Tolppanen, P. (2002). 3D characterization of coarse aggregates. *Engineering Geology* (65), pp. 17–30.

- Lee, J. R., Smith, M. L., & Smith, L. N. (2007). A new approach to the three-dimensional quantification of angularity using image analysis of the size and form of coarse aggregates. *Engineering Geology (91)*, pp. 254–264.
- Lefebvre, M., Gil, S., Glassey, M. A., Baur, C., & Pun, T. (1992). 3D Computer Vision for Agrotics: the Potato Operation an Overview. Conference A: Computer Vision and Applications. *Conference A: Computer Vision and Applications* (pp. pp. 207-210). 11th IAPR International Conference.
- MacLeod, N. (2002). Geometric morphometrics and geological shape-classification systems. *Earth-Science Reviews (59)*, pp. 27-47.
- Maerz, N. H. (1998). Aggregate sizing and shape determination using digital image processing. *Sixth Annual Symposium Proceedings* (pp. pp. 195-203). Missouri: Center For Aggregates Research (ICAR) .
- Marshall, D. (1997). *3D imaging*. Retrieved from Image Acquisition: http://homepages.inf.ed.ac.uk/rbf/CVonline/LOCAL_COPIES/MARSHALL/node8.html
- Marshall, D. (1997). *3D Imaging*. Retrieved 2011, from Image Acquisition: <http://www.cs.cf.ac.uk/Dave/AI2/node174.html>
- Marshall, D. (1997). *3D Imaging*. Retrieved from Image Acquisition: <http://www.cs.cf.ac.uk/Dave/AI2/node174.html>
- Masad, E. (2002). *Image Analysis of Aggregates Samples*. Texas: The University of Texas.
- McAndrew, A. (2004). *Introduction to Digital Image Processing with Matlab*. USA: Thomson Course Technology.
- McClave, J. T., Dietrich II, F. H., & Sincich, T. (1997). *Statistics 7th Ed*. USA: Prentice-Hall Inc.

- Meers, S., & Ward, K. (2009). Face recognition using a time-of-flight camera. *Proceedings of the 2009 Sixth International Conference on Computer Graphics, Imaging and* (pp. 1-6). China: University of Wollongong Research Online.
- Mora, C. F., & Kwan, A. K. (2000). Sphericity, shape factor, and convexity measurement of coarse aggregate for concrete using digital image processing. *Cement and Concrete Research* (30), pp. 351-358.
- Mora, C. F., Kwan, A. K., & Chan, H. C. (1998). Particle Size Distribution Analysis of Coarse Aggregate Using Digital Image Processing. *Cement and Concrete Research* (28), pp. 921-932.
- Neville, A. M. (1995). *Properties of Concrete. (4th ed.)*. England: Longman Ltd.
- Nichols, A. B., & Lange, D. A. (2006). 3D surface image analysis for fracture modeling of cement-based materials. *Cement and Concrete Research* (36), pp. 1098-1107.
- Olm, J., & Gaffney, B. (2010). Stereoscopic 3D. In J. A. Okun, & S. Zwerman, *The VES Handbook of Visual Effects: Industry Standard VFX Practices and Procedures* (pp. 396-406). UK: Elsevier Inc.
- Öztemel, E. (2003). *Yapay Sinir Ağları*. İstanbul: Papatya Yayınları.
- Persson, A. L. (1998). Image analysis of shape and size of fine aggregates. *Engineering Geology* (50), pp. 177-186.
- Peterson, L. E. (2009). *K-Nearest Neighbor*. Retrieved 2011, from Scholarpedia: http://www.scholarpedia.org/article/K-nearest_neighbor
- Pratt, W. K. (2001). *Digital Image Processing: PIKS Inside (3rd ed.)*. New York: John Wiley & Sons, Inc.
- Price, S. (1996, July 4). *Fundamentals: Laser ranging using Time of Flight*. Retrieved 2011, from CVonline: The Evolving, Distributed, Non-Proprietary, On-Line Compendium of Computer Vision:

http://homepages.inf.ed.ac.uk/rbf/CVonline/LOCAL_COPIES/MARBLE/low/fundamentals/laser.htm

- Price, S. (1996). *Fundamentals: Three-dimensional Imaging*. Retrieved from Low Level Vision: Fundamentals: homepages.inf.ed.ac.uk/rbf/CVonline/LOCAL_COPIES/MARBLE/low/fundamentals/3d.htm
- Quiroga, P., & Fowler, D. (2004). *The effect of the aggregate characteristics on the performance of Portland cement concrete*. Texas: ICAR research Report 104-1F.
- Ringbeck, T., & Hagebeuker, B. (2007). A 3D time of flight camera for object detection. *Optical 3-D Measurement Techniques*, 1-11.
- Russ, J. C. (2002). *The Image Processing Handbook (4th ed.)*. North Carolina: CRC Press LLC.
- Sá, J. P. (2001). *Pattern Recognition Concepts, Methods and Applications*. USA: Springer.
- Samadzadegana, F., Azizia, A., Hahn, M., & Lucasa, C. (2005). Automatic 3D object recognition and reconstruction based on neuro-fuzzy modeling. *ISPRS Journal of Photogrammetry and Remote Sensing (59)*, pp. 255-277.
- Schwarte, R. (2001). Dynamic 3D-Vision. *Proceedings Edmo 2001* (pp. pp. 241-248). Vienna: IEEE.
- Schwarte, R., Häusler, G., & Malz, R. W. (2000). Three-Dimensional Imaging Techniques. In B. Jähne, & H. Haußecker, *Computer Vision and Applications* (pp. 196-197). USA: Academic Press.
- Semwogerere, D., & Weeks, E. R. (2005). *Confocal Microscopy*. Taylor & Francis.
- Shapiro, L. G., & C., S. G. (2001). *Computer Vision*. USA: Prentice Hall.
- Shim, S.-O., & Choi, T.-S. (2010). Depth from focus based on combinatorial optimization. *Optics Letters*, 1956-1958.

- Shirai, Y. (1992). 3D Computer Vision and Applications. *Conference A: Computer Vision and Applications* (pp. pp. 236 – 245). Netherlands: 11th IAPR International Conference on (I).
- Soodamani, R., & Liu, Z. Q. (1995). Fuzzy Surface Descriptions For 3-D Machine Vision. *Intelligent Systems for the 21st Century* (pp. pp. 3238 - 324). Vancouver: IEEE International Conference.
- Tam, V. (2007). Aggregate testing using 2nd-, 7th- and 10th-order interpolation polynomials. *Resources, Conservation & Recycling* (52), 39-57.
- Terzaghi, K., & Peck, R. B. (1967). *Soil Mechanics in Engineering Practice* (2nd Ed.). New York: Jhon Wiley and Sons.
- Topal, A. (2001). *Fine aggregate angularity in Turkey in bituminous mixtures*. Izmir: M.Sc Thesis, Natural and Applied Science Institute, Dokuz Eylul University.
- Topal, A. (2008). *Development of new digital image analysis methods for determination of the geometrical properties of aggregates*. Izmir: PhD Thesis (In Turkish), Natural and Applied Science Institute, Dokuz Eylul University.
- Trucco, & Verri, A. (1998). *Introductory Techniques for 3-D Computer Vision*. USA: Prentice Hall.
- Ugurlu, A. (1999). *Agrega - Çimento Hamuru Bağı Üzerine. 2.Ulusal Kırmataş Sempozyumu'99*, (pp. pp. 213-228). İstanbul.
- Ünal, O. (2011). *Agrega*. Retrieved 2011, from Türkiye'nin Kalite Kontrol Portalı: <http://www.kalitekontrol.org/on-sayfa/agrega.html>
- Wadell, H. (1935). Volume, shape, and roundness of quartz particles. *Journal of Geology* (43), pp. 450-480.
- Wang, W. (2006). Image analysis of particles by modified Ferret method best-fit rectangle. *Powder Technology* (165), pp. 1–10.

- Welling, M. (2006). *Fisher Linear Discriminant Analysis*. Retrieved 2011, from Computer Science in Practice: <http://www.cs.huji.ac.il/~csip/Fisher-LDA.pdf>
- Wong, A. K., Rong, L., & Liang, X. (1998). Robotic Vision: 3D Object Recognition and Pose Determination. *Conference on Intelligent Robots and Systems* (pp. pp. 1202 - 1209). Victoria: IEEE/RSJ International Conference.
- Wright, P. J. (1955). A method of measuring the surface texture of aggregate. *Magazine of Concrete Research* (21), pp. 151-160.
- Wu, J., Tillett, R., McFarlane, N., Ju, X., Siebert, J. P., & Schofield, P. (2004). Extracting the three-dimensional shape of live pigs using stereo photogrammetry. *Computers and Electronics in Agriculture* (44), pp. 203-222.
- Wyant, J. C. (2002). White Light Interferometry. *Gaylord Palms Resort and Convention Center*. Florida: AeroSense.
- Wyant, J. C. (2008). *College of Optical Science*. Retrieved from Meeting Papers: http://www.optics.arizona.edu/jcwyant/pdf/meeting_papers/whitelightinterferometry.pdf
- Young, I. T., Gerbrands, J. J., & V., V. L. (1995). *Fundamentals of Image Processing*. Den Haag: Cip-Data Koninklijke Bibliotheek.
- Young, I. T., Gerbrands, J. J., & Vliet, L. J. (1995). *Fundamentals of Image Processing*. Den Haag: Cip-Data Koninklijke Bibliotheek.